Journal Pre-proof

Adiponectin peptide alleviates oxidative stress and NLRP3 inflammasome activation after cerebral ischemia-reperfusion injury by regulating AMPK/GSK-3β

Haixiao Liu, Xun Wu, Jianing Luo, Lei Zhao, Xia Li, Hao Guo, Hao Bai, Wenxing Cui, Wei Guo, Dayun Feng, Yan Qu

PII: S0014-4886(20)30133-3

DOI: https://doi.org/10.1016/j.expneurol.2020.113302

Reference: YEXNR 113302

To appear in: *Experimental Neurology*

Received date: 12 February 2020

Revised date: 20 March 2020

Accepted date: 3 April 2020

Please cite this article as: H. Liu, X. Wu, J. Luo, et al., Adiponectin peptide alleviates oxidative stress and NLRP3 inflammasome activation after cerebral ischemia-reperfusion injury by regulating AMPK/GSK-3β, *Experimental Neurology* (2020), https://doi.org/10.1016/j.expneurol.2020.113302

Adiponectin peptide alleviates oxidative stress and NLRP3 inflammasome activation after cerebral ischemia-reperfusion injury by regulating AMPK/GSK-3β.

Haixiao Liu[1, 2, *], Xun Wu[1, *], Jianing Luo[1, *], Lei Zhao[1], Xia Li[1], Hao Guo[1], Hao Bai[1], Wenxing Cui[1], Wei Guo[1], Dayun Feng[1], Yan Qu[1,#]

1 Department of Neurosurgery, Tangdu Hospital, The Fourth Military Medical University, Xi'an, Shaanxi, China.

2 Department of Pathology, University of Texas Southwestern Medical Center, Dallas, Texas, USA.

[#] Corresponding to Yan Qu, Department of Neurosurgery, Tangdu Hospital, No. 569 Xinsi Road, Xi'an, 710038, China, E-mail: yanqu0123@fmmu.edu.cn, Fax: +86-29-84717556.

[*] Dr. Haixiao Liu, Xun Wu and Jianing Luo contributed equally to this work.

Abstract

The effects of current treatment strategies for ischemic stroke are weakened by ischemia-reperfusion (I/R) injury. Effective treatments targeting I/R injury are still insufficient. Adiponectin (APN), a fat-derived hormone, has a wide range of antioxidative and anti-inflammatory effects. However, the application of APN to the central nervous system is restricted by its limited blood-brain barrier permeability. Therefore, an adiponectin peptide (APNp) was chemically synthesized on the basis of the functional area in the APN structure. The present study was carried out to explore the effect and the underlying mechanism of APNp on I/R injury. A transient middle cerebral artery occlusion (tMCAO) model with C57BL/6J mice was used, and an in vitro oxygen-glucose deprivation and reintroduction (OGD-R) model with primary astrocytes was induced. The results showed that APNp decreased the cerebral infarction volume, alleviated brain edema, improved neurological function and had antioxidative, anti-inflammatory, and antiapoptotic effects against cerebral I/R injury. In addition, APNp upregulated the phosphorylation of AMPK and GSK-3β, promoted the nuclear translocation of Nrf2 and increased the expression of Trx1. The protective effect of APNp was abolished by compound C, a selective AMPK inhibitor, and PX-12, a selective Trx inhibitor. Moreover, APNp

decreased the protein level of TXNIP and suppressed the activation of the NLRP3 inflammasome in astrocytes, which were also reversed by compound C and PX-12. These findings suggest that APNp, as a potential substitute for adiponectin, has a great potential for clinical application in the treatment of acute brain ischemia.

Keywords Adiponectin peptide, cerebral ischemia-reperfusion injury, NLRP3 inflammasome, oxidative stress, AMP-activated protein kinase, thioredoxin

Introduction

Acute stroke is one of the leading causes of mortality and disability worldwide (Donnan et al., 2008; Liu et al., 2011; Liu et al., 2007). Brain ischemia is intractable not only because of the primary injuries caused by ischemia, but also because of the ischemia-reperfusion (I/R) injury, which limits the benefits of reperfusion therapies. Many pathological processes, including oxidative stress and neuroinflammation, are involved in the I/R injury (Dirnagl et al., 1999; Eltzschig and Eckle, 2011; Lo et al., 2003).

Adiponectin (APN) is mainly derived from adipose tissue and is released into circulation (Fasshauer and Bluher, 2015). It has the potential to protect against brain disorders (Jian et al., 2019; Ng et al., 2016; Song et al., 2017). APN promotes the phosphorylation of AMP-activated protein kinase (AMPK) by binding to its receptors, adiponectin receptor 1 (AdipoR1) and adiponectin receptor 2 (AdipoR2) (Kadowaki and Yamauchi, 2005). The upregulation of endogenous AdipoR1 protects against cerebral I/R in diabetic mice in an AMPK- and glycogen synthase kinase-3β (GSK-3β)- dependent manner (Duan et al., 2016).

However, as a 247-amino-acid polypeptide with a molecular weight of 30 kDa, APN has restricted blood-brain barrier (BBB) permeability under physiological conditions.

Intracerebroventricular (i.c.v.) injection and adenovirus-mediated supplementation are the most frequently adopted strategies for administering exogenous APN into brain tissue (Liu et al., 2019a; Miyatake et al., 2015; Nishimura et al., 2008; Wang et al., 2018b). However, it should be acknowledged that i.c.v. injection and virus-mediating upregulation are not clinically compatible, which severely restricts their translation into clinical practice. Therefore, in the present study, an APN peptide (APNp) (amino acid sequence: NH_2-LQVYGDGLHNGLYADNVN-COOH (Li et al., 2017; Lyzogubov et al., 2009)), regarded as a potential APN substitute, was chemically synthesized on the basis of the functional area in APN's globular domain (Fruebis et al., 2001; Rak et al., 2017; Ujiie et al., 2006).

Nucleotide-binding and oligomerization domain-like receptor family pyrin domain-containing 3 (NLRP3) is an intracellular sensor that detects changes in the microenvironment and responds to the endogenous danger signals, which leads to the formation and activation of the NLRP3 inflammasome (Swanson et al., 2019). The NLRP3 inflammasome, consisting of NOD-like receptor, NLRP3, apoptosis-associated speck-like protein containing a caspase recruitment domain (ASC) and caspase-1, has been demonstrated to be involved in the inflammation responses in a variety of pathological conditions, including those caused by I/R

injury (Fann et al., 2013; Mangan et al., 2018; Minutoli et al., 2016).

The generation of reactive oxygen species (ROS), which are produced in mitochondria by the electron transport chain under physiological conditions and induce oxidative stress under pathological conditions, is considered one of the most important regulating factors of NLRP3 inflammasome activation (Tschopp and Schroder, 2010). The thioredoxin (Trx) system is one of the main intracellular antioxidant systems, and it detoxifies ROS and protects cells from oxidative damage (Cheng et al., 2011). The thioredoxin-interacting protein (TXNIP) represents the intersection of oxidative stress and inflammasome activation (Zhou et al., 2010). As one of the critical mechanisms in I/R injury, the overload of ROS not only induces oxidative stress damage but also mediates inflammation and apoptosis (Bolanos et al., 2009; Forrester et al., 2018). However, the role of Trx/TXNIP, ROS, and the NLRP3 inflammasome in the protection of APN against cerebral I/R injury remains unclear.

The present study was designed to explore the antioxidative and anti-inflammatory mechanism of APNp in an in vivo transient middle cerebral artery occlusion (tMCAO) model and an in vitro oxygen-glucose deprivation and reintroduction (OGD-R) model. The roles of AMPK/GSK-3β/nuclear factor erythroid 2-related factor 2 (Nrf2) and Trx1/TXNIP/ROS/NLRP3

were explored.

Materials and Methods

Animals and ethics

Healthy adult male C57BL/6J mice weighing 20-25 g were provided by the experimental animal center of the Fourth Military Medical University. The mice were housed in a pathogen-free conditions under a stable temperature (23°C), a stable humidity level (60%), and a 12 h light/dark cycle, and given free access to food and water. The experiments were approved by the Ethics Committee of the Fourth Military Medical University and performed according to *The Guide for the Care and Use of Laboratory Animals* (National Institutes of Health Publication, No. 85-23, revised 1996). The pain suffered by the animals was relieved as much as possible.

Reagents

APNp and fluorescein (FITC)-labelled APNp were chemically synthesized by Sangon Biotech Co. (Shanghai, China). 1-methylpropyl 2-imidazolyl disulfide (PX-12) was purchased from SelleckChem (Houston, USA). Compound C (CC) (ab146597) was purchased from Abcam (Cambridge, UK). The dimethyl sulfoxide (DMSO) was purchased from Sigma-Aldrich (St.

Louis, MO, USA).

The 8-hydroxy-2-deoxyguanosine (8-OHdG) and 3-nitrotyrosine (3-NT) enzyme-linked immunosorbent assay (ELISA) kits were purchased from Cell Biolabs (San Diego, USA). The kits used to measure glutathione peroxidase (GSH-Px), superoxide dismutase (SOD), and malondialdehyde (MDA) levels were purchased from the Institute of Jiancheng Bioengineering (Nanjing, Jiangsu, China). Bicinchoninic acid (BCA) protein assay kit was purchased from Beyotime (Shanghai, China). The nuclear and cytoplasmic extraction kit was purchased from Thermo Fisher (TX, USA). Fluoro-Jade C (FJC) was purchased from Millipore (Temecula, USA). The terminal deoxynucleotidyl transferase UTP nick-end labeling (TUNEL) kit was purchased from Roche (Mannheim, Germany). The 2,3,5-triphenyltetrazoliumchloride (TTC), ROS fluorescent probe-dihydroethidium (DHE), and 4,6-diamino-2-phenylindole (DAPI) were purchased from Sigma-Aldrich (St. Louis, MO, USA).

Rabbit polyclonal antibodies against cleaved caspase-3 (ab2302) and interleukin (IL)-1β (ab9722), rabbit monoclonal antibody against AdipoR1 (ab126611), and goat polyclonal antibody against glial fibrillary acidic protein (GFAP) (ab53554) were purchased from Abcam (Cambridge, UK). Mouse monoclonal antibody against neuronal nuclei (NeuN) (MAB377) were purchased

from Millipore (Temecula, USA). Rabbit polyclonal antibodies against nucleotide binding and oligomerization domain-like receptor family pyrin domain-containing 3 (NLRP3) (sc-66846), ASC (sc-22514-R), IL-18 (sc-7954), goat polyclonal antibody against caspase-1 p20 (sc-1597), and mouse monoclonal antibody against Nrf2 (sc-365949) were purchased from Santa Cruz Biotechnology (Santa Cruz, CA, USA). Rabbit monoclonal antibodies against B-cell lymphoma 2 (Bcl-2) (2870), Bcl-2 associated X (Bax) (14796), Trx1 (2429S), TXNIP (14715S), AMPK (2532S), phospho-AMPK (Thr172) (D4D6D), GSK-3β (12456), phospho-GSK-3β (Ser9) (5558), and histone H3 (4499S) were purchased from Cell Signaling Technology (Beverly, MA, USA). Rabbit polyclonal antibody against β-actin (AC006) was purchased from ABclonal Biotech (College Park, Maryland, USA).

The HRP-conjugated rabbit anti-goat, goat anti-rabbit, and goat anti-mouse secondary antibodies were purchased from Bioworld Co. (Shanghai, China). The Cy3-Conjugated goat anti-rabbit (CW0159), goat anti-mouse (CW0145), and donkey anti-goat (CW0216), and FITC-Conjugated donkey anti-rabbit (CW0219) and goat anti-mouse (CW0113) secondary antibodies were purchased from the ComWin Biotech Co. (Beijing, China).

Experimental design

First, with the purpose of evaluating the protective effect of APNp and exploring the underlying mechanisms, mice were randomly and blindly separated into different groups: (1) the sham group, (2) tMCAO group, (3) Tmcao + vehicle group, and (4) tMCAO + APNp group. Second, with the purpose of evaluating the effect of Trx and AMPK on the protective mechanisms, PX-12 and CC were used, which created the need for two more groups: (1) the tMCAO + APNp + PX-12 group, and (2) tMCAO + APNp + CC group.

With the purpose of investigating the effects of APNp on primary astrocytes, 5 groups were generated: (1) the control group, (2) OGD-R group, (3) OGD-R + APNp group, (4) OGD-R + APNp + PX-12 group, and (5) OGD-R + APNp + CC group.

tMCAO model and treatments

The tMCAO model was generated by a skillful researcher following a previously reported method (Matsumura et al., 2019) and according to the IMPROVE guidelines (Percie du Sert et al., 2017). Briefly, after the mice were anesthetized with a mixture of isoflurane (3% induction and 1.5% maintenance, v/v) in 30% oxygen and 70% nitrous oxide, a midline neck incision was made to expose the right common carotid artery (CCA) bifurcation. Then, the right external carotid artery (ECA) was ligated and dissected, and a nylon suture with a smooth, rounded tip was

inserted into the right internal carotid artery through the bifurcation of the right ECA stump and the right CCA for a distance of 10 ± 0.5 mm to block the right middle cerebral artery. Reperfusion was allowed 90 min later by suture withdrawal. Similar operations were performed on the sham animals, except that the suture was inserted for a distance of less than 8 mm to avoid occlusion. The animals were kept warm using a heating plate to maintain body temperature at 36.5 - 37.5°C during the surgery. Meloxicam was given as analgesic after the surgery, and 0.2 ml of normal saline (with 5% glucose) was administered as nutritional support twice per day after the surgery.

APNp was diluted to a concentration of 5 mg/ml with 0.9% saline solution and intraperitoneally injected at a dose of 20 μg/(g body weight) immediately after occlusion. For treatment of the tMCAO + APNp + PX-12 group and the tMCAO + APNp + CC group, the PX-12 (25 μg/(g body weight)) or CC (2 μg/(g body weight)) was dissolved in DMSO, diluted with normal saline and administered through tail vein injection immediately after the occlusion was created. The final concentration of DMSO was 1%. The control mice were injected with the same volume of the vehicle (**Fig 1a**).

Neurological scores

The neurological deficit score was evaluated by an observer blinded to the study design

using the previously reported Garcia scoring method (Garcia et al., 1995; Matsumura et al., 2019; Zhao et al., 2017). In brief, the evaluation consists of 6 tests: (1) spontaneous activity, (2) symmetry in the movement of four limbs, (3) forepaw outstretching, (4) climbing, (5) body proprioception, and (6) response to vibrissae touch. Each of these tests was graded with a 0-3 score. In this system, a higher evaluated score indicates a better neurological function, while a low score indicates a functional deficit.

Cerebral infarct volume

Staining with 2,3,5-triphenyltetrazolium chloride (TTC) was performed to evaluate the cerebral infarct size. After being anesthetized with 2% pentobarbital sodium, the mice were transcardially perfused with 40 ml of 0.1 M phosphate buffer (PBS) (pH=7.4). Then, the brains were removed and sectioned into 1-mm thick slices. The sections were incubated at 37°C for 20 min with 2% TTC dissolved in PBS. The tissues that suffered I/R injury remained white, whereas the other tissues were stained brick red. The slices were photographed and then analyzed blindly using Image-Pro Plus 6.0 to calculate the infarct volume. The infarction proportion was calculated as ((Red area on left-Red area on right) / Red area on left)×100%.

Brain water content

Brain water content was measured to evaluate the severity of brain edema using the standard wet-dry method (Hatashita et al., 1988). The mice were sacrificed 72 h after I/R was induced, and the right cerebrums were removed and immediately weighed (wet weight). After being dehydrated in an oven (105°C) for 72 h, the dry samples were weighed (dry weight). The brain water content was calculated as ((wet weight - dry weight)/wet weight) ×100%.

Evaluating the penetrability of APNp to the BBB

FITC-labeled APNp was injected intraperitoneally into mice at a dose of 20 μg/(g body weight). The animals under anesthesia were perfused transcardially with 40 ml of ice-cold PBS after 24 h. Then, the brain was removed, frozen immediately on dry ice, and sliced into 15-μm thick coronal slices using a freezing microtome (CM 1950, Leica, German). The slices were incubated with DAPI staining solution (5 μg/ml) for 10 min at 37°C, washed with PBS, and then observed under a laser scanning confocal microscope (A1 Si, Nikon, Japan).

ROS staining

DHE staining was conducted to evaluate the production of reactive oxygen species and oxidative stress in injured tissues 24 h after I/R induction. Under anesthesia, the animals were perfused transcardially with ice-cold PBS. Then, the brains were removed, frozen immediately on

dry ice, and sliced into 15-μm thick slices. The slices were dyed with DHE for 30 min and observed under a laser scanning confocal microscope (A1 Si, Nikon, Japan). Five areas in the cortex in the penumbra (**Fig 1b c**) were randomly chosen to calculate the average positive cell count (Liu et al., 2019b).

Assays of MDA content and SOD and GSH-Px activity levels

The tissues in the penumbra area were collected 24 h after I/R was induced using a previously published method (Ashwal et al., 1998). The collected tissues were lysed and homogenized in lysis buffer (Beyotime Institute of Biotechnology, Shanghai, China) on ice for 30 min and centrifuged (12,000 rpm) at 4 °C for 15 min to obtain the supernatant. Then, the levels of MDA and the activity of two oxidative stress-related enzymes, SOD and GSH-Px, were detected following the instructions of commercial kits. The principle of the MDA level assay was that malondialdehyde and thiobarbituric acid react under acid conditions at high temperatures, and the maximum absorbance peak of the generated 3,5,5'-three methyloxazole-2,4-diketone (λ = 532 nm) is measured. SOD activity was tested by the WST-1 method (λ = 450 nm). The GSH-Px activity was tested by measuring the reduction in NADPH in the reaction system (λ = 412 nm). The optical density (OD) values were detected by a SpectraMax M2 spectrometer (Molecular Devices,

Sunnyvale, CA, USA).

Evaluation of 3-NT and 8-OHdG levels

The concentrations of 3-NT and 8-OHdG were measured following the instructions of commercial ELISA kits 24 h after I/R induction. In brief, the samples and standards were added to a 96-well plate and then incubated with primary antibodies overnight at 4°C, appropriate secondary antibodies for 1 h at room temperature, and a substrate solution for 15 min at room temperature in the dark. Finally, the reaction terminating solution was added into each well, and the absorbance in each well was measured by a SpectraMax M2 spectrometer. A standard curve was generated and used to determine the levels of 3-NT and 8-OHdG in the samples.

TUNEL assay

Cellular apoptosis was detected by TUNEL staining. Brains were removed after being transcardially perfused with 40 ml of ice-cold PBS and 40 ml of ice-cold 4% paraformaldehyde (PH=7.4) (PFA) solution under anesthesia and were stored in 4% paraformaldehyde at 4 °C for 2 h. Then, they were dehydrated in 10%, 20%, and 30% sucrose solutions dissolved in PBS until they sank. The dehydrated tissues were sliced into 25-μm-thick coronal slices and incubated with 0.3% hydrogen peroxide for 30 min at room temperature, 0.25% pancreatin for 45 min at 37°C,

TUNEL reaction solution for 60 min at 37°C, and DAPI staining solution for 10 min at 37°C. Each of these steps was followed by washing with PBS 3 times for 5 min each time. The slices were photographed by a confocal microscope and analyzed blindly by Image-Pro Plus 6.0. The apoptotic index was reflected by the ratio of TUNEL-positive cells to DAPI-positive cells.

Fluoro-Jade C staining

Fluoro-Jade C (F-JC) staining was performed to detect neuronal degeneration 72 h after reperfusion. Selected brain slices (**Fig 1b c**) were incubated with 1% NaOH in 80% ethanol for 5 min and rehydrated with 70% ethanol for 2 min and distilled water for 2 min. Then, they were incubated with 0.06% $KMnO_4$ for 10 min, rinsed with distilled water for 3 min, and incubated with 0.0001% F-JC solution for 15 min. Finally, the slices were washed with distilled water 3 times for 1 min each time. The slices were observed, and the F-JC-positive neurons were counted and calculated.

Immunofluorescence staining

The tissues were perfused, collected, fixed, dehydrated, and sliced as described above. The slices were treated with 0.3% Triton X-100 for 30 min at room temperature, blocked with 10 % donkey serum for 60 min at room temperature, and incubated overnight with rabbit polyclonal

anti-AdipoR1 (1:200, Abcam), goat polyclonal anti-GFAP (1:200, Abcam), or mouse monoclonal anti-NeuN (1:200, Millipore) primary antibodies at 4°C. Next, the slices were incubated with the appropriate secondary antibody for 2 h at room temperature and with DAPI (5 μg/ml, Sigma-Aldrich) for 10 min at 37°C. Each of these steps was followed by washing with PBS 3 times for 5 mins each time. The average number of positive cells in five randomly chosen views in the penumbra was calculated.

Western blot analysis

The samples in the penumbra area and the cultured cells were lysed and homogenized in lysis buffer containing 1% protease inhibitor and 1% phosphatase inhibitor (Roche, Mannheim, Germany) on ice for 30 min and then sonicated. Nuclear and cytoplasmic proteins were extracted using a nuclear and cytoplasmic extraction kit. Protein concentrations were measured using a BCA protein assay kit. Equal amounts of protein samples (30 μg per lane) were separated in 8-15% SDS-polyacrylamide gels and transferred onto polyvinylidene difluoride (PVDF) membranes (Millipore Corporation, Billerica, MA, USA). The membranes were blocked with 5% nonfat milk in Tris-buffered saline and Tween 20 (pH 7.6) (TBST) for 120 min at room temperature, and incubated overnight at 4°C with primary rabbit polyclonal antibody against Bax (14796, 1:1000),

Bcl-2 (2870, 1:1000), cleaved caspase-3 (ab2302, 1:1000), cleaved caspase-9(Asp330)(7237, 1:1000), Trx 1 (2429S, 1:1000), TXNIP (14715S, 1:1000), NLRP3 (sc-66846, 1:500), ASC (sc-22514-R, 1:500), caspase-1 p20 (sc-1597, 1:500), IL-1β (ab9722, 1:1000), IL-18 (sc-7954, 1:500), AMPK(2532S, 1:1000), phospho-AMPK (D4D6D, 1:1000), GSK-3β (12456, 1:1000), phospho-GSK-3β (5558, 1:1000), Nrf2 (sc-365949, 1:500), β-actin (AC006, 1:1000), histone H3 (4499S, 1:1000). Then they were incubated with the appropriate HRP-conjugated secondary antibody (1:10000) for 1.5 h at room temperature. Finally, the membranes were visualized by a Bio-Rad imaging system (Bio-Rad, Hercules, CA, USA).

Transmission electron microscopy observations

The ultrastructural changes in the neurons in the penumbra were observed by transmission electron microscopy using a previously reported method (Li et al., 2017). Briefly, animals were anesthetized and perfused with PBS and PFA 72 h after I/R induction. The cortical tissues in the penumbra region were cut perpendicular to the long axis and trimmed into 1.5mm×1.5mm×3mm blocks. Then, the specimens were fixed in 4% glutaraldehyde for 12 h, postfixed in 1% osmium tetroxide for 1 h, dehydrated in graded ethanol, embedded in resin, and cut into 80 nm sections by an ultramicrotome (Leica, Vienna, Austria). The ultrathin sections were fixed on 200-slot grids

coated with pioloform membrane and observed with a JEM-1400 electron microscope (JEOL, Tokyo, Japan). The images of the micrographs were captured by a charge-coupled device camera (Olympus, Tokyo, Japan).

Cell culture and the OGD-R model

Primary astrocytes were obtained from the brains of postnatal (P1 to P2) C57BL/6J mice using a previously described method (Feng et al., 2015; Han et al., 2018). Briefly, mice were sacrificed, and the brain cortices were removed quickly and placed into ice-cold Hank's magnesium- and calcium-free solution. The tissues were digested with trypsin-EDTA after the large blood vessels and membranes were removed. Then, the cells were resuspended in Dulbecco's modified Eagle's medium (DMEM) (Corning, MT10013CV) with 10% fetal bovine serum (FBS) (Gibco, 10099141), 100 U/ml penicillin and 100 U/ml streptomycin, planted on poly-L-lysine precoated cell culture flasks, and cultured in a humidified incubator (5% CO2/95% air). After 7-8 days, the flasks were shaken for 20 h at 220 rpm to obtain purified astrocytes. Astrocytes were harvested at 10 days and reseeded at a density of 2.5×10^5 cells/cm^2 for the following experiments.

The OGD-R model was induced following a previously reported method (Bernstein et al.,

2020; Liu et al., 2019b; Shan et al., 2019). Briefly, the culture medium was replaced with glucose-free DMEM, and the cells were transferred to a hypoxic chamber (95% N_2, 5% CO_2) at 37°C. Three hours later, the glucose-free DMEM was replaced by normal DMEM, and oxygen was reintroduced to the cells quickly. Then, the cells were treated with APNp, CC, PX-12, or the vehicle according to the study design. APNp was dissolved in DMSO and diluted into a final concentration of 50 μM with culture medium (DMSO ≤ 0.01%) immediately prior to use. The culture medium with 0.01% DMSO was used in the control group. PX-12 and CC were dissolved in DMSO and used at the concentration of 20 μM and 10 μM, respectively. The cells were harvested at 24 h after OGD-R.

Statistical analysis

The statistical analyses were conducted blindly using the GraphPad Prism 6 (GraphPad Software, San Diego, CA, USA) and SPSS 20.0 (IBM, Chicago, IL, USA). Neurological scores were expressed as median and 25th - 75th percentile values. They were analyzed by Kruskal–Wallis one-way analysis of variance (ANOVA) on ranks, followed by Tukey's post hoc analysis. Other data were expressed as means ± standard deviation (SD) and analyzed by one-way ANOVA followed by Tukey's post hoc analysis. Multiple comparisons were performed using Tukey's

honest significant difference post hoc test after a one-way ANOVA was completed. One-way ANOVAs, as well as Bonferroni multiple comparison tests, were adopted for intergroup comparisons. $P < 0.05$ was considered statistically significant.

Results

APNp alleviated the neurological deficit, brain edema, infarct size, and cellular apoptosis after cerebral I/R in mice.

The APN peptide was chemically synthesized in the present study on the basis of the globular domain, the functional area of the APN at the C-terminal end of its amino acid sequence(Fruebis et al., 2001; Rak et al., 2017; Ujiie et al., 2006). FITC-labeled APNp was intraperitoneally administered to the mice. The BBB penetrability of APNp was observed and verified under a laser scanning confocal microscope 24 h after the APNp injection (**Fig 1d**). Then, the effects of the APNp on cerebral I/R were explored in mice.

Twenty animals in each group were observed for 14 days to evaluate the postinjury survival rate. The survival rates in the sham, I/R, I/R + vehicle, and I/R + APNp groups were 20, 10, 9, and 13 out of 20, respectively (**Fig 1e**). Six mice in each group were maintained for 4 days to

evaluate the postinjury neurological functions. The neurological score in the I/R and I/R + vehicle groups decreased significantly compared with the sham group, while the APNp administration significantly improved neurological functions after I/R (**Fig 1f**). In addition, the brain edema and cerebral infarction volume were also alleviated by APNp after I/R induction (**Fig 1g-i**).

Then, apoptosis in the penumbra tissue was evaluated. APNp administration significantly decreased the apoptosis index 24 h after I/R induction (vs. the I/R + vehicle group, $P < 0.05$) (**Fig 2a b**). In addition, the increase in the protein levels of Bax/Bcl-2 and cleaved caspase-3 induced by I/R were reversed by the APNp treatment (**Fig 2c-e**).

APNp ameliorated oxidative stress after cerebral I/R in mice.

The capacity of APNp to treat oxidative stress was evaluated 24 h after I/R induction. The DHE-positive cells in the I/R + APNp group decreased dramatically (vs. the I/R + vehicle group, $P < 0.05$) (**Fig 3a b**). In addition, the activity levels of SOD and GSH-Px, two main oxidative stress-related enzymes; the level of MDA, a product of lipid peroxidation; the level of 3-NT, a product of tyrosine oxidation; and the level of 8-OHdG, one of the most sensitive DNA damage markers of oxidative stress injury, were measured. The impairments to the SOD and GSH-Px

activity levels and the increase in MDA, 3-NT and 8-OHdG levels in the penumbra area after I/R induction were significantly alleviated by the APNp treatment (**Fig 3c-g**).

APNp inhibited the activity of the NLRP3 inflammasome after cerebral I/R, which were regulated by AMPK phosphorylation.

The effects of APNp on NLRP3 inflammasome activation at 72 h after cerebral I/R induction were measured to explore their protective mechanism. The protein levels of TXNIP, NLRP3, ASC, caspase-1 p20, IL-1β, and IL-18 increased remarkably, while the protein level of Trx1 decreased significantly in the I/R and I/R + venicle groups (vs. the sham group, $P < 0.05$). APNp administration reversed this trend to promote Trx1 downregulation and NLRP3 inflammasome activation (**Fig 4a-f**). Then, PX-12, a Trx1 inhibitor, was introduced into this study as a negative control. The suppression effects of APNp against the upregulation of TXNIP, NLRP3, ASC, and caspase-1 p20 were reversed by the addition of PX-12 (**Fig 4g-l**). Moreover, F-JC staining showed that PX-12 decreased the neuron-protecting effect of APNp after I/R (**Fig 4m n**), which suggested that Trx1 was indispensable to the protective mechanism of APNp.

The activation of AMPK plays a critical role in the physiology and pathology activity of adiponectin(Iwabu et al., 2010; Kadowaki and Yamauchi, 2005; Miller et al., 2008). GSK-3β is

another important signal transduction molecule activated upon AdipoR1 induction(Duan et al., 2016; Guo et al., 2015; Wang et al., 2006). In the present study, we investigated the phosphorylation of AMPK and GSK-3β. The protein levels of p-AMPK (Thr172)/AMPK and p-GSK-3β (Ser9)/GSK-3β in the penumbra were significantly upregulated by APNp (**Fig 5a-c**). Moreover, CC, a selective AMPK inhibitor, significantly decreased the phosphorylation of GSK-3β, downregulated the protein level of Trx1, and upregulated the protein level of TXNIP (**Fig 5d-h**).

Furthermore, the protective effect of APNp can be reversed by AMPK inhibition and Trx1 inhibition. The alleviation of cerebral infarction and brain edema by APNp was inhibited by PX-12 and CC (**Fig 6a-c**). The increase of NeuN-positive cells in the penumbra area after APNp treatment was also inhibited by PX-12 and CC (**Fig 6d-e**). PX-12 and CC impaired the antioxidative effect of APNp. DHE staining showed that the decrease in ROS production after APNp administration was abolished by PX-12 and CC (**Fig 6f g**). In addition, PX-12 and CC significantly increased the levels of MDA and decreased the activity of SOD and GSH-Px (**Fig 6h-j**). The accumulation of ROS is observed during mitochondrial dysfunction, which leads to cell death(Navarro-Yepes et al., 2014). Thus, ultrastructural changes in mitochondria and

endoplasmic reticulum in neurons were observed. Neurons of the APNp + I/R group were nearly intact, with more mitochondrial cristae and nearly normal endoplasmic reticulum morphology. However, swollen mitochondria, loss of mitochondrial cristae, and morphological changes in the endoplasmic reticulum were observed in the neurons of the I/R, I/R + APNp + PX-12, and I/R + APNp + CC groups (**Fig 6k**). In addition, the protein levels of Bax/Bcl-2 and cleaved caspase-3 were upregulated when PX-12 and CC were administered together with APNp (**Fig 6l-n**).

APNp alleviated NLRP3 inflammasome activation in primary astrocytes by regulating AMPK phosphorylation.

Adiponectin acts through two receptors: AdipoR1 and AdipoR2(Tanabe et al., 2015). AdipoR1 is upregulated after brain ischemia(Thundyil et al., 2012). However, it remains unclear that which type of cells adiponectin mainly targets after I/R. The cellular localization of AdipoR1 in the penumbra was investigated in the present study. A greater amount of AdipoR1 was expressed in astrocytes (**Fig 7b**), although AdipoR1 was also expressed in neurons (**Fig 7a**).

Thus, the effects of APNp on AMPK phosphorylation and NLRP3 inflammasome activation were investigated in primary astrocytes. The phosphorylation of AMPK (Thr172) and GSK-3β (Ser9) and nuclear translocation of Nrf2 were notably promoted by APNp and were

downregulated by CC (**Fig 7c e-g**). These preliminary results warranted a particular and in-depth study into the intracellular signal transduction pathway induced by APNp treatment. In addition, APNp administration ameliorated the increase in the protein levels of TXNIP, NLRP3, ASC, caspase-1 p20, IL-1β, and IL-18, and notably alleviated the decrease in Trx1 after OGD-R. However, PX-12 and CC inhibited this effect of APNp (**Fig 7d h-k**). These results suggested that APNp could inhibit the activation of the NLRP3 inflammasome in the OGD-R-treated astrocytes in an AMPK phosphorylation-dependent manner.

Discussion

In the present study, it was revealed that (1) APNp can cross the BBB and ameliorated oxidative stress and inflammation, inhibit cellular apoptosis, reduce infarct size, alleviate brain edema, and enhance neurological function after cerebral I/R injury in mice. (2) APNp can also inhibit the activation of the NLRP3 inflammasome after cerebral I/R injury in mice, and this effect can be regulated by AMPK (Thr172) phosphorylation. The protective effects of APNp were abolished by the Trx1 inhibitor and AMPK inhibitor. (3) APNp inhibited the activation of the NLRP3 inflammasome in astrocytes by regulating the phosphorylation of AMPK (Thr172)

and GSK-3β (Ser9), the nuclear translocation of Nrf2, and the levels of Trx1 and TXNIP after OGD-R. These results verified the protective effect of APNp, revealed its underlying mechanisms, and provided a new strategy for the clinical applications of adiponectin (**Fig 8**).

A series of complex mechanisms are involved in the pathological process of cerebral ischemia. Excitotoxicity and ionic imbalance, oxidative stress and nitrosative stress, apoptosis-associated and autophagy-associated cell death, and necrosis all contribute to this process(Dirnagl et al., 1999; Eltzschig and Eckle, 2011; Lo et al., 2003). In clinical practice, intravenous thrombolysis within the initial 4.5 h after onset of injury is the mainstay of acute ischemia stroke therapy(Catanese et al., 2017). However, the ROS, a key mediator of tissue damage, is produced abundantly upon reperfusion, which creates a tremendous problem for the use of this strategy(Lo et al., 2003). The complicated mechanism of ischemia injury and reperfusion injury makes finding better treatments for cerebral ischemia an arduous endeavor.

Adiponectin is an insulin-sensitizing protein secreted by adipose cells to a high plasma concentration(Tilg and Moschen, 2006). APN regulates the metabolism of glucose and lipids(Fang and Judd, 2018; Wang and Scherer, 2016). In addition, it has protective effects in a variety of cardiovascular diseases, including myocardial I/R and inflammatory cardiomyopathy

byc inhibiting inflammation and oxidative/nitrative stress(Bobbert et al., 2011; Tao et al., 2007; Wang et al., 2014). It has been reported that APN potentially confers cerebral protection through an endothelial nitric oxide synthase-related mechanism and AMPK pathway after stroke(Liu et al., 2019a; Nishimura et al., 2008). However, in these studies, the exogenous APN was added in an adenovirus-mediated manner or by lateral ventricle injection, which are not clinically practical methods. Therefore, APNp, as a potential substitute that mimics the protective effect of APN, has been chemically synthesized. Our data suggest that APNp had potential to ameliorate oxidative stress, neuroinflammation, and apoptosis in mice with induced cerebral I/R injury. These findings were consistent with those of previous studies(Bai et al., 2018; Li et al., 2017; Liu et al., 2019a; Wang et al., 2018a; Yue et al., 2016).

The function of APN depends on the binding of APN to its receptors (AdipoR1, AdipoR2, and T-cadherin), which activates numerous signaling molecules, including AMPK, p38-MAPK, JNK, PPARα and the NF-κB transcription factor. These receptors are widely expressed in the brain(Fang and Judd, 2018; Thundyil et al., 2012). The expression of AdipoR1 in mouse cortical neurons is much higher than that of AdipoR2(Thundyil et al., 2012). AdipoR1 is also expressed in microglia and astrocytes(Zhao et al., 2018). However, the precise roles of these receptors as

potential therapeutic targets in cerebral I/R injury remain unclear. In the present study, most AdipoR1 colocalized with astrocytes, indicating that the anti-inflammatory effect of APN might be achieved by acting on astrocytes.

AMPK, a central regulator of energy homeostasis, is activated by the phosphorylation of Thr172 in its T-loop (activation loop)(Steinberg and Carling, 2019). APN protected against cell apoptosis induced by myocardial I/R injury by activating AMPK(Shibata et al., 2005). In addition, APN attenuated neuronal apoptosis after neonatal hypoxia-ischemia by activating the AdipoR1/APPL1/LKB1/AMPK pathway(Xu et al., 2018). Moreover, the upregulation of endogenous APN and AdipoR1 induced by Chikusetsu saponin IVa pretreatment protected against focal cerebral I/R in diabetic mice by enhancing the phosphorylation of AMPK (Thr172) and GSK-3β (Ser9)(Duan et al., 2016).

GSK-3β plays a critical role in the resistance of oxidative stress and apoptosis-related neuron damage. Phosphorylation of GSK-3β at tyrosine-216 enhances the enzymatic activity of GSK-3, while phosphorylation at serine-9 significantly decreases its activity(Beurel et al., 2015). In the present study, APNp alleviated neuron damage by promoting the activity of AMPK and inhibiting the activity of GSK-3β.

The nuclear accumulation of Nrf2, an antioxidant transcription factor that regulates a series of downstream neuroprotective proteins, including Trx1, can be promoted by AMPK activation(Joo et al., 2016; Yang et al., 2015). LPS-induced inflammation can be alleviated by the phosphorylation of AMPK/GSK-3β and the upregulation of the Nrf2 pathway(Lv et al., 2017). Nrf-2 also plays a protective role in cerebral I/R injury by inhibiting the formulation of the NLPR3 inflammasome by regulating the Trx1/TXNIP complex(Hou et al., 2018). In the present study, our data showed that the nuclear translocation of Nrf2 was enhanced by APNp-induced AMPK activation.

The Trx system is a main intracellular antioxidant systems, which detoxifies ROS and protects cells from oxidative damage(Cheng et al., 2011). Our previous study demonstrated that the administration of recombinant human Trx1 exerted an antioxidative and antiapoptotic effect against I/R injury(Wang et al., 2015). As an intersection of oxidative stress and inflammasome activation, TXNIP, also known as vitamin D3 upregulated protein 1 (VDUP1) or thioredoxin-binding protein-2 (TBP-2), was essential in post I/R inflammatory injury and oxidative damage(Zhou et al., 2010). ROS promoted the expression of TXNIP, the dissociation of TXNIP from thioredoxin, and the binding of TXNIP to NLRP3, which led to the activation of the

NLRP3 inflammasome(Nasoohi et al., 2018; Zhou et al., 2010). Excessive TXNIP also decreased the activity and expression of Trx1(Watanabe et al., 2010). In contrast, TXNIP deficiency inhibited the activation of the NLRP3 inflammasome. AMPK could regulate the TXNIP level by promoting the phosphorylation and degradation of TXNIP and modulating the activity of carbohydrate response element-binding protein (ChREBP). Our work verified that Trx insufficiency and TXNIP overload are important initiators of NLRP3 inflammasome activation and oxidative stress injury after cerebral I/R injury. APNp maintained the function of Trx/TXNIP system.

As a cytosolic macromolecular complex, the NLRP inflammasome recruits and cleaves precursor caspase-1 into caspase-1 p20 via proximity-induced autoactivation, and therefore induces the cleaving of pro-IL-1β and pro-IL-18 into their active forms(Swanson et al., 2019). The mature IL-1β and IL-18, as pro-inflammatory cytokines, can be released into the extracellular environment and induce neuroinflammation. In the present study, this pro-inflammatory process was inhibited by APNp in an AMPK- and Trx- dependent manner.

Apoptosis, as a type of programmed cell death pathway, is controlled by the Bcl-2 family. The balance of proapoptotic proteins, such as Bax, and antiapoptotic proteins, such as Bcl-2,

control the mitochondrial apoptosis pathway(Singh et al., 2019). When liberated from the antiapoptotic Bcl-2 family members, Bax could cause mitochondrial membrane permeabilization and activate caspase-9, which could activate caspase-3(Fricker et al., 2018; Hotchkiss et al., 2009). The ultrastructure of mitochondria in neurons and the levels of proteins in the mitochondrial apoptosis pathway were investigated in this study, which confirmed the antiapoptotic effect of APNp.

It is of great significance to explore the effects of treatments at certain time points or time periods considering that the injury mechanism evolves over time. In the present study, the effects of APNp on oxidative stress and neuroinflammation after cerebral I/R injury were observed. However, the development of these two mechanisms over time is not completely synchronized. Oxidative stress occurs very early after the onset of stroke. ROS, a key mediator of oxidative stress, is generated abundantly during cerebral ischemia/reperfusion and induces oxidative stress rapidly (Chen et al., 2011; Granger and Kvietys, 2015; Lo et al., 2003). Multiple cells and multiple mechanisms are involved in the inflammatory response. The glial cells are activated and inflammatory responses are initiated within several hours after stroke. However, this is just the first stage of the neuroinflammation. The inflammatory response evolves gradually after initiation and peaks several days after injury (Dirnagl et al., 1999; Heiss et al., 1999; Jayaraj et al., 2019; Petrovic-Djergovic et al., 2016; Stoll et al., 1998). Thus, in the present study, the oxidative stress was tested 24 h after injury, while the inflammation was tested 72 h after injury. Besides, animals suffered the most severe damage

2-4 days post-surgery. In the present study, mice have a higher mortality rate on the third day after surgery **(Fig 1e),** and the differences in neurological scores between the I/R + vehicle and I/R + APNp group became more significant at 72 hours post-surgery **(Fig 1f)**. It was also shown in the previous studies that the deference of brain water content between the MCAO group and MCAO + treatment group might continue to increase in the first 72 hours after surgery (Austin et al., 2019; Cheng et al., 2015; Huang et al., 2013). Therefore, the brain water content was tested at 72 hours after surgery in the present study. However, the protective mechanism of APNp at other post-injury time points are also quite significant, which is worthy to be further explored in the future.

In summary, APNp, a substitute for APN, regulated the activity of AMPK and GSK-3β and alleviated the ROS/Trx1/TXNIP-related oxidative stress, inflammation, and apoptosis induced by I/R in the mice. The ameliorating effect of APNp against NLRP3 inflammasome activation was realized in an AMPK-dependent manner. Our findings suggest that APNp has great potential for clinical application in the treatment of acute brain ischemia. However, evidence about a particular intracellular signal transduction mechanism of the APNp/AdipoR signal remains insufficient. The underlying mechanisms are to be revealed before APNp can be transformed for clinical use.

Funding

This work was supported by the National Natural Science Foundation of China [grant numbers 81571215, 81630027].

Acknowledgments

The authors thank the editors from American Journal Experts for their help with professional language editing.

Conflict of interest

The authors have no conflicts of interest to declare.

Reference

Ashwal, S., Tone, B., Tian, H.R., Cole, D.J., Pearce, W.J., 1998. Core and penumbral nitric oxide synthase activity during cerebral ischemia and reperfusion. Stroke 29, 1037-1046; discussion 1047.

Austin, V., Ku, J.M., Miller, A.A., Vlahos, R., 2019. Ischaemic stroke in mice induces lung inflammation but not acute lung injury. Sci Rep 9, 3622.

Bai, H., Zhao, L., Liu, H., Guo, H., Guo, W., Zheng, L., Liu, X., Wu, X., Luo, J., Li, X., Gao, L., Feng, D., Qu, Y., 2018. Adiponectin confers neuroprotection against cerebral ischemia-reperfusion injury through activating the cAMP/PKA-CREB-BDNF signaling. Brain Res Bull 143, 145-154.

Bernstein, D.L., Gajghate, S., Reichenbach, N.L., Winfield, M., Persidsky, Y., Hendt, N.A., Rom, S., 2020. let-7g counteracts endothelial dysfunction and ameliorating neurological functions in mouse ischemia/reperfusion stroke model. Brain Behav Immun.

Beurel, E., Grieco, S.F., Jope, R.S., 2015. Glycogen synthase kinase-3 (GSK3): regulation, actions, and diseases. Pharmacol Ther 148, 114-131.

Bobbert, P., Scheibenbogen, C., Jenke, A., Kania, G., Wilk, S., Krohn, S., Stehr, J., Kuehl, U., Rauch, U., Eriksson, U., Schultheiss, H.P., Poller, W., Skurk, C., 2011. Adiponectin expression in patients with inflammatory cardiomyopathy indicates favourable outcome and inflammation control. Eur Heart J 32, 1134-1147.

Bolanos, J.P., Moro, M.A., Lizasoain, I., Almeida, A., 2009. Mitochondria and reactive oxygen and nitrogen species in neurological disorders and stroke: Therapeutic implications. Adv Drug Deliv Rev 61, 1299-1315.

Catanese, L., Tarsia, J., Fisher, M., 2017. Acute Ischemic Stroke Therapy Overview. Circ Res 120, 541-558.

Chen, H., Yoshioka, H., Kim, G.S., Jung, J.E., Okami, N., Sakata, H., Maier, C.M., Narasimhan, P., Goeders, C.E., Chan, P.H., 2011. Oxidative stress in ischemic brain damage: mechanisms of cell death and potential molecular targets for neuroprotection. Antioxid Redox Signal 14, 1505-1517.

Cheng, Q., Zhang, Z., Zhang, S., Yang, H., Zhang, X., Pan, J., Weng, L., Sha, D., Zhu, M., Hu, X., Xu, Y., 2015. Human umbilical cord mesenchymal stem cells protect against ischemic brain injury in mouse by regulating peripheral immunoinflammation. Brain Res 1594, 293-304.

Cheng, Z., Zhang, J., Ballou, D.P., Williams, C.H., Jr., 2011. Reactivity of thioredoxin as a protein thiol-disulfide oxidoreductase. Chem Rev 111, 5768-5783.

Dirnagl, U., Iadecola, C., Moskowitz, M.A., 1999. Pathobiology of ischaemic stroke: an integrated view. Trends Neurosci 22, 391-397.

Donnan, G.A., Fisher, M., Macleod, M., Davis, S.M., 2008. Stroke. Lancet 371, 1612-1623.

Duan, J., Yin, Y., Cui, J., Yan, J., Zhu, Y., Guan, Y., Wei, G., Weng, Y., Wu, X., Guo, C., Wang, Y., Xi, M., Wen, A., 2016. Chikusetsu Saponin IVa Ameliorates Cerebral Ischemia Reperfusion Injury in Diabetic Mice via

Adiponectin-Mediated AMPK/GSK-3beta Pathway In Vivo and In Vitro. Mol Neurobiol 53, 728-743.

Eltzschig, H.K., Eckle, T., 2011. Ischemia and reperfusion--from mechanism to translation. Nat Med 17, 1391-1401.

Fang, H., Judd, R.L., 2018. Adiponectin Regulation and Function. Compr Physiol 8, 1031-1063.

Fann, D.Y., Lee, S.Y., Manzanero, S., Chunduri, P., Sobey, C.G., Arumugam, T.V., 2013. Pathogenesis of acute stroke and the role of inflammasomes. Ageing Res Rev 12, 941-966.

Fasshauer, M., Bluher, M., 2015. Adipokines in health and disease. Trends Pharmacol Sci 36, 461-470.

Feng, D., Guo, B., Liu, G., Wang, B., Wang, W., Gao, G., Qin, H., Wu, S., 2015. FGF2 alleviates PTSD symptoms in rats by restoring GLAST function in astrocytes via the JAK/STAT pathway. Eur Neuropsychopharmacol 25, 1287-1299.

Forrester, S.J., Kikuchi, D.S., Hernandes, M.S., Xu, Q., Griendling, K.K., 2018. Reactive Oxygen Species in Metabolic and Inflammatory Signaling. Circ Res 122, 877-902.

Fricker, M., Tolkovsky, A.M., Borutaite, V., Coleman, M., Brown, G.C., 2018. Neuronal Cell Death. Physiol Rev 98, 813-880.

Fruebis, J., Tsao, T.S., Javorschi, S., Ebbets-Reed, D., Erickson, M.R., Yen, F.T., Bihain, B.E., Lodish, H.F., 2001. Proteolytic cleavage product of 30-kDa adipocyte complement-related protein increases fatty acid oxidation in muscle and causes weight loss in mice. Proc Natl Acad Sci U S A 98, 2005-2010.

Garcia, J.H., Wagner, S., Liu, K.F., Hu, X.J., 1995. Neurological deficit and extent of neuronal necrosis attributable to middle cerebral artery occlusion in rats. Statistical validation. Stroke 26, 627-634; discussion 635.

Granger, D.N., Kvietys, P.R., 2015. Reperfusion injury and reactive oxygen species: The evolution of a concept. Redox Biol 6, 524-551.

Guo, F., Jiang, T., Song, Y., Wei, H., Wang, F., Liu, L., Ma, L., Yin, H., Wang, Q., Xiong, L., 2015. Electroacupuncture attenuates cerebral ischemia-reperfusion injury in diabetic mice through adiponectin receptor 1-mediated phosphorylation of GSK-3beta. Mol Neurobiol 51, 685-695.

Han, B., Zhang, Y., Zhang, Y., Bai, Y., Chen, X., Huang, R., Wu, F., Leng, S., Chao, J., Zhang, J.H., Hu, G., Yao, H., 2018. Novel insight into circular RNA HECTD1 in astrocyte activation via autophagy by targeting MIR142-TIPARP: implications for cerebral ischemic stroke. Autophagy 14, 1164-1184.

Hatashita, S., Hoff, J.T., Salamat, S.M., 1988. Ischemic brain edema and the osmotic gradient between blood and brain. J Cereb Blood Flow Metab 8, 552-559.

Heiss, W.D., Thiel, A., Grond, M., Graf, R., 1999. Which targets are relevant for therapy of acute ischemic stroke? Stroke 30, 1486-1489.

Hotchkiss, R.S., Strasser, A., McDunn, J.E., Swanson, P.E., 2009. Cell death. N Engl J Med 361, 1570-1583.

Hou, Y., Wang, Y., He, Q., Li, L., Xie, H., Zhao, Y., Zhao, J., 2018. Nrf2 inhibits NLRP3 inflammasome activation through regulating Trx1/TXNIP complex in cerebral ischemia reperfusion injury. Behav Brain Res 336, 32-39.

Huang, J., Li, Y., Tang, Y., Tang, G., Yang, G.Y., Wang, Y., 2013. CXCR4 antagonist AMD3100 protects blood-brain barrier integrity and reduces inflammatory response after focal ischemia in mice. Stroke 44, 190-197.

Iwabu, M., Yamauchi, T., Okada-Iwabu, M., Sato, K., Nakagawa, T., Funata, M., Yamaguchi, M., Namiki, S., Nakayama, R., Tabata, M., Ogata, H., Kubota, N., Takamoto, I., Hayashi, Y.K., Yamauchi, N., Waki, H., Fukayama, M., Nishino, I., Tokuyama, K., Ueki, K., Oike, Y., Ishii, S., Hirose, K., Shimizu, T., Touhara, K., Kadowaki, T., 2010. Adiponectin and AdipoR1 regulate PGC-1alpha and mitochondria by Ca(2+) and AMPK/SIRT1. Nature 464, 1313-1319.

Jayaraj, R.L., Azimullah, S., Beiram, R., Jalal, F.Y., Rosenberg, G.A., 2019. Neuroinflammation: friend and foe for ischemic stroke. J Neuroinflammation 16, 142.

Jian, M., Kwan, J.S., Bunting, M., Ng, R.C., Chan, K.H., 2019. Adiponectin suppresses amyloid-beta oligomer (AbetaO)-induced inflammatory response of microglia via AdipoR1-AMPK-NF-kappaB signaling pathway. J Neuroinflammation 16, 110.

Joo, M.S., Kim, W.D., Lee, K.Y., Kim, J.H., Koo, J.H., Kim, S.G., 2016. AMPK Facilitates Nuclear Accumulation of Nrf2 by Phosphorylating at Serine 550. Mol Cell Biol 36, 1931-1942.

Kadowaki, T., Yamauchi, T., 2005. Adiponectin and adiponectin receptors. Endocr Rev 26, 439-451.

Li, X., Guo, H., Zhao, L., Wang, B., Liu, H., Yue, L., Bai, H., Jiang, H., Gao, L., Feng, D., Qu, Y., 2017. Adiponectin attenuates NADPH oxidase-mediated oxidative stress and neuronal damage induced by cerebral ischemia-reperfusion injury. Biochim Biophys Acta Mol Basis Dis 1863, 3265-3276.

Liu, B., Liu, J., Wang, J., Sun, F., Jiang, S., Hu, F., Wang, D., Liu, D., Liu, C., Yan, H., 2019a. Adiponectin Protects Against Cerebral Ischemic Injury Through AdipoR1/AMPK Pathways. Front Pharmacol 10, 597.

Liu, H., Wu, X., Luo, J., Wang, X., Guo, H., Feng, D., Zhao, L., Bai, H., Song, M., Liu, X., Guo, W., Li, X., Yue, L., Wang, B., Qu, Y., 2019b. Pterostilbene Attenuates Astrocytic Inflammation and Neuronal Oxidative Injury After Ischemia-Reperfusion by Inhibiting NF-kappaB Phosphorylation. Front Immunol 10, 2408.

Liu, L., Wang, D., Wong, K.S., Wang, Y., 2011. Stroke and stroke care in China: huge burden, significant workload, and a national priority. Stroke 42, 3651-3654.

Liu, M., Wu, B., Wang, W.Z., Lee, L.M., Zhang, S.H., Kong, L.Z., 2007. Stroke in China: epidemiology, prevention, and management strategies. Lancet Neurol 6, 456-464.

Lo, E.H., Dalkara, T., Moskowitz, M.A., 2003. Mechanisms, challenges and opportunities in stroke. Nat Rev Neurosci 4, 399-415.

Lv, H., Liu, Q., Wen, Z., Feng, H., Deng, X., Ci, X., 2017. Xanthohumol ameliorates lipopolysaccharide (LPS)-induced acute lung injury via induction of AMPK/GSK3beta-Nrf2 signal axis. Redox Biol 12, 311-324.

Lyzogubov, V.V., Tytarenko, R.G., Thotakura, S., Viswanathan, T., Bora, N.S., Bora, P.S., 2009. Inhibition of new vessel growth in mouse model of laser-induced choroidal neovascularization by adiponectin peptide II. Cell Biol Int 33, 765-771.

Mangan, M.S.J., Olhava, E.J., Roush, W.R., Seidel, H.M., Glick, G.D., Latz, E., 2018. Targeting the NLRP3 inflammasome in inflammatory diseases. Nat Rev Drug Discov 17, 588-606.

Matsumura, K., Kumar, T.P., Guddanti, T., Yan, Y., Blackburn, S.L., McBride, D.W., 2019. Neurobehavioral Deficits After Subarachnoid Hemorrhage in Mice: Sensitivity Analysis and Development of a New Composite Score. J Am Heart Assoc 8, e011699.

Miller, E.J., Li, J., Leng, L., McDonald, C., Atsumi, T., Bucala, R., Young, L.H., 2008. Macrophage migration inhibitory factor stimulates AMP-activated protein kinase in the ischaemic heart. Nature 451, 578-582.

Minutoli, L., Puzzolo, D., Rinaldi, M., Irrera, N., Marini, H., Arcoraci, V., Bitto, A., Crea, G., Pisani, A., Squadrito, F., Trichilo, V., Bruschetta, D., Micali, A., Altavilla, D., 2016. ROS-Mediated NLRP3 Inflammasome Activation in Brain, Heart, Kidney, and Testis Ischemia/Reperfusion Injury. Oxid Med Cell Longev 2016, 2183026.

Miyatake, Y., Shiuchi, T., Ueta, T., Taniguchi, Y., Futami, A., Sato, F., Kitamura, T., Tsutsumi, R., Harada, N., Nakaya, Y., Sakaue, H., 2015. Intracerebroventricular injection of adiponectin regulates locomotor activity in rats. J Med Invest 62, 199-203.

Nasoohi, S., Ismael, S., Ishrat, T., 2018. Thioredoxin-Interacting Protein (TXNIP) in Cerebrovascular and Neurodegenerative Diseases: Regulation and Implication. Mol Neurobiol 55, 7900-7920.

Navarro-Yepes, J., Zavala-Flores, L., Anandhan, A., Wang, F., Skotak, M., Chandra, N., Li, M., Pappa, A., Martinez-Fong, D., Del Razo, L.M., Quintanilla-Vega, B., Franco, R., 2014. Antioxidant gene therapy against neuronal cell death. Pharmacol Ther 142, 206-230.

Ng, R.C., Cheng, O.Y., Jian, M., Kwan, J.S., Ho, P.W., Cheng, K.K., Yeung, P.K., Zhou, L.L., Hoo, R.L., Chung, S.K., Xu, A., Lam, K.S., Chan, K.H., 2016. Chronic adiponectin deficiency leads to Alzheimer's disease-like cognitive impairments and pathologies through AMPK inactivation and cerebral insulin resistance in aged mice. Mol Neurodegener 11, 71.

Nishimura, M., Izumiya, Y., Higuchi, A., Shibata, R., Qiu, J., Kudo, C., Shin, H.K., Moskowitz, M.A., Ouchi, N., 2008. Adiponectin prevents cerebral ischemic injury through endothelial nitric oxide synthase dependent mechanisms. Circulation 117, 216-223.

Percie du Sert, N., Alfieri, A., Allan, S.M., Carswell, H.V., Deuchar, G.A., Farr, T.D., Flecknell, P., Gallagher, L., Gibson, C.L., Haley, M.J., Macleod, M.R., McColl, B.W., McCabe, C., Morancho, A., Moon, L.D., O'Neill, M.J., Perez de Puig, I., Planas, A., Ragan, C.I., Rosell, A., Roy, L.A., Ryder, K.O., Simats, A., Sena, E.S., Sutherland, B.A., Tricklebank, M.D., Trueman, R.C., Whitfield, L., Wong, R., Macrae, I.M., 2017. The IMPROVE Guidelines (Ischaemia Models: Procedural Refinements Of in Vivo Experiments). J Cereb Blood Flow Metab 37, 3488-3517.

Petrovic-Djergovic, D., Goonewardena, S.N., Pinsky, D.J., 2016. Inflammatory Disequilibrium in Stroke. Circ Res 119, 142-158.

Rak, A., Mellouk, N., Froment, P., Dupont, J., 2017. Adiponectin and resistin: potential metabolic signals affecting hypothalamo-pituitary gonadal axis in females and males of different species. Reproduction 153, R215-r226.

Shan, Y., Tan, S., Lin, Y., Liao, S., Zhang, B., Chen, X., Wang, J., Deng, Z., Zeng, Q., Zhang, L., Wang, Y., Hu, X., Qiu, W., Peng, L., Lu, Z., 2019. The glucagon-like peptide-1 receptor agonist reduces inflammation and blood-brain barrier breakdown in an astrocyte-dependent manner in experimental stroke. J Neuroinflammation 16, 242.

Shibata, R., Sato, K., Pimentel, D.R., Takemura, Y., Kihara, S., Ohashi, K., Funahashi, T., Ouchi, N., Walsh, K., 2005. Adiponectin protects against myocardial ischemia-reperfusion injury through AMPK- and COX-2-dependent mechanisms. Nat Med 11, 1096-1103.

Singh, R., Letai, A., Sarosiek, K., 2019. Regulation of apoptosis in health and disease: the balancing act of BCL-2 family proteins. Nat Rev Mol Cell Biol 20, 175-193.

Song, J., Choi, S.M., Whitcomb, D.J., Kim, B.C., 2017. Adiponectin controls the apoptosis and the expression of tight junction proteins in brain endothelial cells through AdipoR1 under beta amyloid toxicity. Cell Death Dis 8, e3102.

Steinberg, G.R., Carling, D., 2019. AMP-activated protein kinase: the current landscape for drug development. Nat Rev Drug Discov 18, 527-551.

Stoll, G., Jander, S., Schroeter, M., 1998. Inflammation and glial responses in ischemic brain lesions. Prog Neurobiol 56, 149-171.

Swanson, K.V., Deng, M., Ting, J.P., 2019. The NLRP3 inflammasome: molecular activation and regulation to therapeutics. Nat Rev Immunol 19, 477-489.

Tanabe, H., Fujii, Y., Okada-Iwabu, M., Iwabu, M., Nakamura, Y., Hosaka, T., Motoyama, K., Ikeda, M., Wakiyama, M., Terada, T., Ohsawa, N., Hato, M., Ogasawara, S., Hino, T., Murata, T., Iwata, S., Hirata, K., Kawano, Y., Yamamoto, M., Kimura-Someya, T., Shirouzu, M., Yamauchi, T., Kadowaki, T., Yokoyama, S., 2015. Crystal structures of the human adiponectin receptors. Nature 520, 312-316.

Tao, L., Gao, E., Jiao, X., Yuan, Y., Li, S., Christopher, T.A., Lopez, B.L., Koch, W., Chan, L., Goldstein, B.J., Ma, X.L., 2007. Adiponectin cardioprotection after myocardial ischemia/reperfusion involves the reduction of oxidative/nitrative stress. Circulation 115, 1408-1416.

Thundyil, J., Pavlovski, D., Sobey, C.G., Arumugam, T.V., 2012. Adiponectin receptor signalling in the brain. Br J Pharmacol 165, 313-327.

Tilg, H., Moschen, A.R., 2006. Adipocytokines: mediators linking adipose tissue, inflammation and immunity. Nat Rev Immunol 6, 772-783.

Tschopp, J., Schroder, K., 2010. NLRP3 inflammasome activation: The convergence of multiple signalling pathways on ROS production? Nat Rev Immunol 10, 210-215.

Ujiie, H., Oritani, K., Kato, H., Yokota, T., Takahashi, I., Maeda, T., Masaie, H., Ichii, M., Kamada, Y., Tamura, S., Kihara, S., Funahashi, T., Tomiyama, Y., Kanakura, Y., 2006. Identification of amino-terminal region of adiponectin as a physiologically functional domain. J Cell Biochem 98, 194-207.

Wang, B., Guo, H., Li, X., Yue, L., Liu, H., Zhao, L., Bai, H., Liu, X., Wu, X., Qu, Y., 2018a. Adiponectin Attenuates Oxygen-Glucose Deprivation-Induced Mitochondrial Oxidative Injury and Apoptosis in Hippocampal HT22 Cells via the JAK2/STAT3 Pathway. Cell Transplant 27, 1731-1743.

Wang, B., Tian, S., Wang, J., Han, F., Zhao, L., Wang, R., Ning, W., Chen, W., Qu, Y., 2015. Intraperitoneal administration of thioredoxin decreases brain damage from ischemic stroke. Brain Res 1615, 89-97.

Wang, S., Li, D., Huang, C., Wan, Y., Wang, J., Zan, X., Yang, B., 2018b. Overexpression of adiponectin alleviates intracerebral hemorrhage-induced brain injury in rats via suppression of oxidative stress. Neurosci Lett 681, 110-116.

Wang, Y., Lam, J.B., Lam, K.S., Liu, J., Lam, M.C., Hoo, R.L., Wu, D., Cooper, G.J., Xu, A., 2006. Adiponectin modulates the glycogen synthase kinase-3beta/beta-catenin signaling pathway and attenuates mammary tumorigenesis of MDA-MB-231 cells in nude mice. Cancer Res 66, 11462-11470.

Wang, Y., Wang, X., Lau, W.B., Yuan, Y., Booth, D., Li, J.I., Scalia, R., Preston, K., Gao, E., Koch, W., Ma, X.L., 2014. Adiponectin inhibits tumor necrosis factor-alpha-induced vascular inflammatory response via caveolin-mediated ceramidase recruitment and activation. Circ Res 114, 792-805.

Wang, Z.V., Scherer, P.E., 2016. Adiponectin, the past two decades. J Mol Cell Biol 8, 93-100.

Watanabe, R., Nakamura, H., Masutani, H., Yodoi, J., 2010. Anti-oxidative, anti-cancer and anti-inflammatory actions by thioredoxin 1 and thioredoxin-binding protein-2. Pharmacol Ther 127, 261-270.

Xu, N., Zhang, Y., Doycheva, D.M., Ding, Y., Zhang, Y., Tang, J., Guo, H., Zhang, J.H., 2018. Adiponectin attenuates neuronal apoptosis induced by hypoxia-ischemia via the activation of AdipoR1/APPL1/LKB1/AMPK pathway in neonatal rats. Neuropharmacology 133, 415-428.

Yang, Y., Jiang, S., Yan, J., Li, Y., Xin, Z., Lin, Y., Qu, Y., 2015. An overview of the molecular mechanisms and novel roles of Nrf2 in neurodegenerative disorders. Cytokine Growth Factor Rev 26, 47-57.

Yue, L., Zhao, L., Liu, H., Li, X., Wang, B., Guo, H., Gao, L., Feng, D., Qu, Y., 2016. Adiponectin Protects against Glutamate-Induced Excitotoxicity via Activating SIRT1-Dependent PGC-1alpha Expression in HT22 Hippocampal Neurons. Oxid Med Cell Longev 2016, 2957354.

Zhao, L., Chen, S., Sherchan, P., Ding, Y., Zhao, W., Guo, Z., Yu, J., Tang, J., Zhang, J.H., 2018. Recombinant CTRP9 administration attenuates neuroinflammation via activating adiponectin receptor 1 after intracerebral hemorrhage in mice. J Neuroinflammation 15, 215.

Zhao, L., Liu, H., Yue, L., Zhang, J., Li, X., Wang, B., Lin, Y., Qu, Y., 2017. Melatonin Attenuates Early Brain Injury via the Melatonin Receptor/Sirt1/NF-kappaB Signaling Pathway Following Subarachnoid Hemorrhage in Mice. Mol Neurobiol 54, 1612-1621.

Zhou, R., Tardivel, A., Thorens, B., Choi, I., Tschopp, J., 2010. Thioredoxin-interacting protein links oxidative stress to inflammasome activation. Nat Immunol 11, 136-140.

Figure Legends

Fig 1: Protocol of in vivo experiment, BBB permeability of APNp, and the alleviating effect of APNp on survival rate, neurological deficits, brain edema, and cerebral infarction after I/R. **(a)** Experimental protocol of the in vivo study. The red diamonds represent the surgical procedure. **(b c)** Schematic diagram of the location of the penumbra area. The sketch in (b) is referenced from Page 77, The Mouse Brain in Stereotaxic Coordinates (second edition), 2001, ACADEMIC PRESS. **(d)** Representative images of FITC-labeled APNp in mice's brain 24h after it's intraperitoneally administrated. Scale bar is 50 μm in zoom-in images and 100μm in other images. **(e)** The post-injury 14-day survival rate. Values are represented as survival percentage. **(f)** The Neurological scores at 2 h, 1d, 2d, 3d, and 4d after reperfusion. **(g)** The brain water content of the injured side cerebrums at 72h after reperfusion. **(h i)** Representative images and statistical analysis of TTC staining, which reflect the effect of APNp on the cerebral infarct volumes 24h after I/R. Values are represented as mean ± SD, n=6 for each group except n=20 for survival rate assessment. $^{**}P < 0.01$ vs. sham group, $^{\#\#}P < 0.01$ vs. I/R + vehicle group.

Fig 2: The anti-apoptosis effects of APNp against I/R injury. **(a b)** Representative images and

statistical analysis of TUNEL stained cortex in the penumbra 24 h after I/R. Scale bar is 50 μm. **(c-e)** The anti-apoptosis effects of APNp. Representative western blot images and statistical analysis of the protein levels of Bax, Bcl-2, and cleaved caspase-3 are shown. Values are represented as mean ± SD, n = 6 for each group. $^{**}P < 0.01$ vs. sham group, $^{\#\#}P < 0.01$ vs. I/R + vehicle group.

Fig 3: The anti-oxidative stress effects of APNp against I/R injury. **(a b)** Representative images and statistical analysis of DHE staining, which indicates the production of reactive oxygen species. Scale bar is 50 μm. **(c-g)** The effects of APNp on the levels of MDA, the activity of SOD and GSH-Px, and the concentrations of 3-NT and 8-OHdG 24h after I/R. Values are represented as mean ± SD, n=6 for each group. $^{**}P < 0.01$ vs. sham group, $^{\#\#}P < 0.01$ vs. I/R + vehicle group.

Fig 4: The inhibiting effects of APNp on NLRP3 inflammasome activation at 72h after I/R injury, which are regulated by Trx and TXNIP. **(a-f)** The inhibiting effect of APNp against NLRP3 inflammasomes after I/R. Representative western blot images and statistical analysis of the protein levels of Trx, TXNIP, NLRP3, ASC, and caspase-1 p20 are shown. **(g-l)** PX-12 abolished

the NLRP3 inflammasome inhibiting effect of APNp. The protein level of Trx is down-regulated by PX-12. Whereas, the protein levels of TXNIP, NLRP3, ASC, and caspase-1 p20 are up-regulated by PX-12, compared to the I/R + APNp group. **(m n)** Representative images and statistical analysis of F-JC staining 72h after I/R, which reflex the neuronal degeneration. Scale bar is 50 μm. Values are represented as mean ± SD, n=6 for each group. $^{**}P < 0.01$ vs. sham group, $^{\#\#}P < 0.01$ vs. I/R group, $^{\$\$}P < 0.01$ vs. I/R + APNp group.

Fig 5: The role of AMPK in the protective effect of APNp. **(a-c)** The phosphorylations of AMPK and Gsk-3β are up-regulated by APNp. Representative western blot images and statistical analysis are shown. Then, CC, a selective AMPK inhibitor, is used to explore the role of AMPK in the APNp's Trx/TXNIP regulating effect. **(d-h)** CC counteracted the Trx up-regulating and TXNIP down-regulating effect of APNp. Representative western blot images and statistical analysis are shown. Values are represented as mean ± SD, n=6 for each group. $^{*}P < 0.05$ vs. sham group, $^{**}P < 0.01$ vs. sham group, $^{\#\#}P < 0.01$ vs. I/R group, $^{\$\$}P < 0.01$ vs. I/R + APNp group.

Fig 6: The roles of AMPK and Trx in the protective effect of APNp. PX-12 and CC abolish the

protective effect of APNp on cerebral infarction, brain edema, oxidative stress, mitochondria impairment, and neuron damage. **(a b)** Representative images and statistical analysis of TTC staining. **(c)** Brain water content. **(d e)** Representative images of NeuN staining and NeuN positive cell count. Scale bar is 50 μm. **(f g)** Representative images and statistical analysis of DHE staining. Scale bar is 50 μm. **(h-j)** The level of MDA and the activities of SOD and GSH-Px 24h after I/R. **(k)** Representative ultrastructure of neurons in the penumbra. k1b-k5b are the enlarged images of k1a-k5a. Scale bar is 2 μm in k1a-k5a and 1 μm in k1b-k5b. Arrows indicate the mitochondria. **(l-n)** Representative western blot images and statistical analysis of the protein level of Bax, Bcl-2, and cleaved caspase-3. Values are represented as mean ± SD. n=6 for each group. $^{**}P < 0.01$ vs. sham group $^{\#\#}P < 0.01$ vs. I/R group, $^{\$}P < 0.05$ vs. I/R + APNp group, $^{\$\$}P < 0.01$ vs. I/R + APNp group.

Fig 7: APNp's anti-inflammation effect in primary astrocyte after OGD-R**. (a)** Representative immunofluorescence images indicate that a handful of AdipoR1 is expressed in neurons. Scale bar is 50 μm. **(b)** AdipoR1 is highly expressed in astrocytes. Scale bar is 50 μm. Then, the primary astrocytes are cultured to test the APNp's effect. **(c e-g)** The phosphorylation levels of

AMPK and Gsk-3β are detected by western blot. The nuclear translocation of Nrf2 is evaluated by nuclear-cytoplasmic extraction followed by western blot. Histone H3 and β-actin are used as loading controls for nuclear protein and cytoplasmic protein respectively. **(d h-n)** The protein levels of Trx/TXNIP and NLRP3 inflammasome activation in astrocyte. The representative western blot images and statistical analysis of the protein level are shown. n=6 for each group. Values are represented as mean ± SD, n=6 for each group except n=8 for cell viability and LDH release assessment. $^{**}P < 0.01$ vs. control group, $^{\#\#}P < 0.01$ vs. OGD group, $^{\$\$}P < 0.01$ vs. OGD + APNp group.

Fig 8: Signaling pathway of APNp's protective effect against cerebral I/R injury which is suggested in the present study. APNp binds to the adiponectin receptor, thus promotes the phosphorylation of AMPK and Gsk-3β, which reduces Gsk-3β's inhibition to Nrf2's function. The nuclear translocation of Nrf2 promotes the expression of Trx, which inhibits ROS production and oxidative stress. Trx also binds to TXNIP thus inhibits the activation of NLRP3 inflammasome. As a result, the neuroinflammation is inhibited. Other intracellular molecules might also be involved in this mechanism, which deserves further exploration.

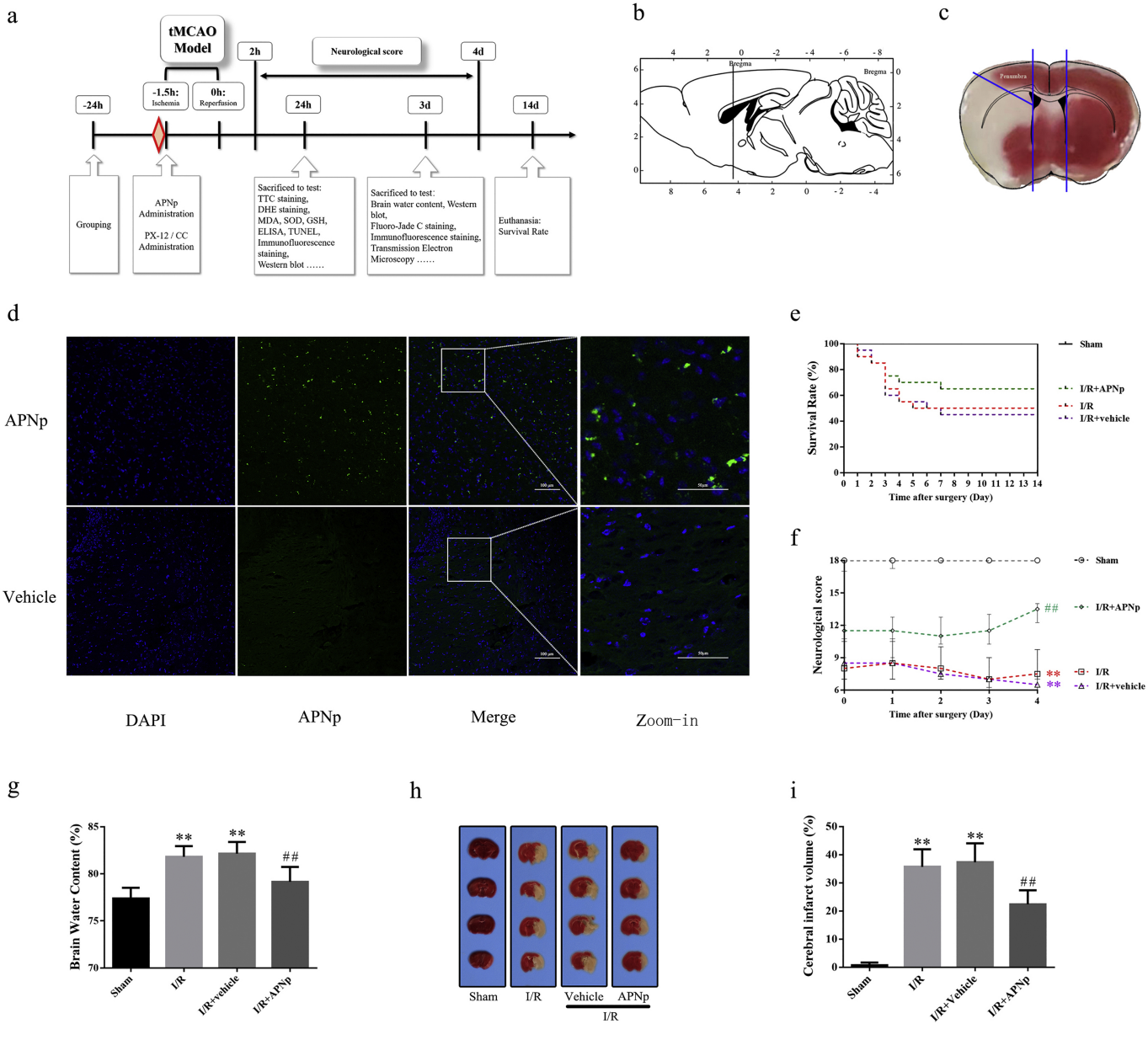
a
tMCAO Model
2h
Neurological score
4d
-1.5h: Ischemia
0h: Reperfusion
-24h
24h
3d
14d
Grouping
APNp Administration
PX-12 / CC Administration
Sacrificed to test: TTC staining, DHE staining, MDA, SOD, GSH, ELISA, TUNEL, Immunofluorescence staining, Western blot ……
Sacrificed to test: Brain water content, Western blot, Fluoro-Jade C staining, Immunofluorescence staining, Transmission Electron Microscopy ……
Euthanasia: Survival Rate
b
Bregma
Bregma
c
Penumbra
d
APNp
Vehicle
DAPI
APNp
Merge
Zoom-in
e
Survival Rate (%)
Time after surgery (Day)
Sham
I/R+APNp
I/R
I/R+vehicle
f
Neurological score
Time after surgery (Day)
Sham
I/R+APNp
I/R
I/R+vehicle
##
**
**
g
Brain Water Content (%)
Sham
I/R
I/R+vehicle
I/R+APNp
**
**
##
h
Sham
I/R
Vehicle
APNp
I/R
i
Cerebral infarct volume (%)
Sham
I/R
I/R+Vehicle
I/R+APNp
**
**
##

Figure 1

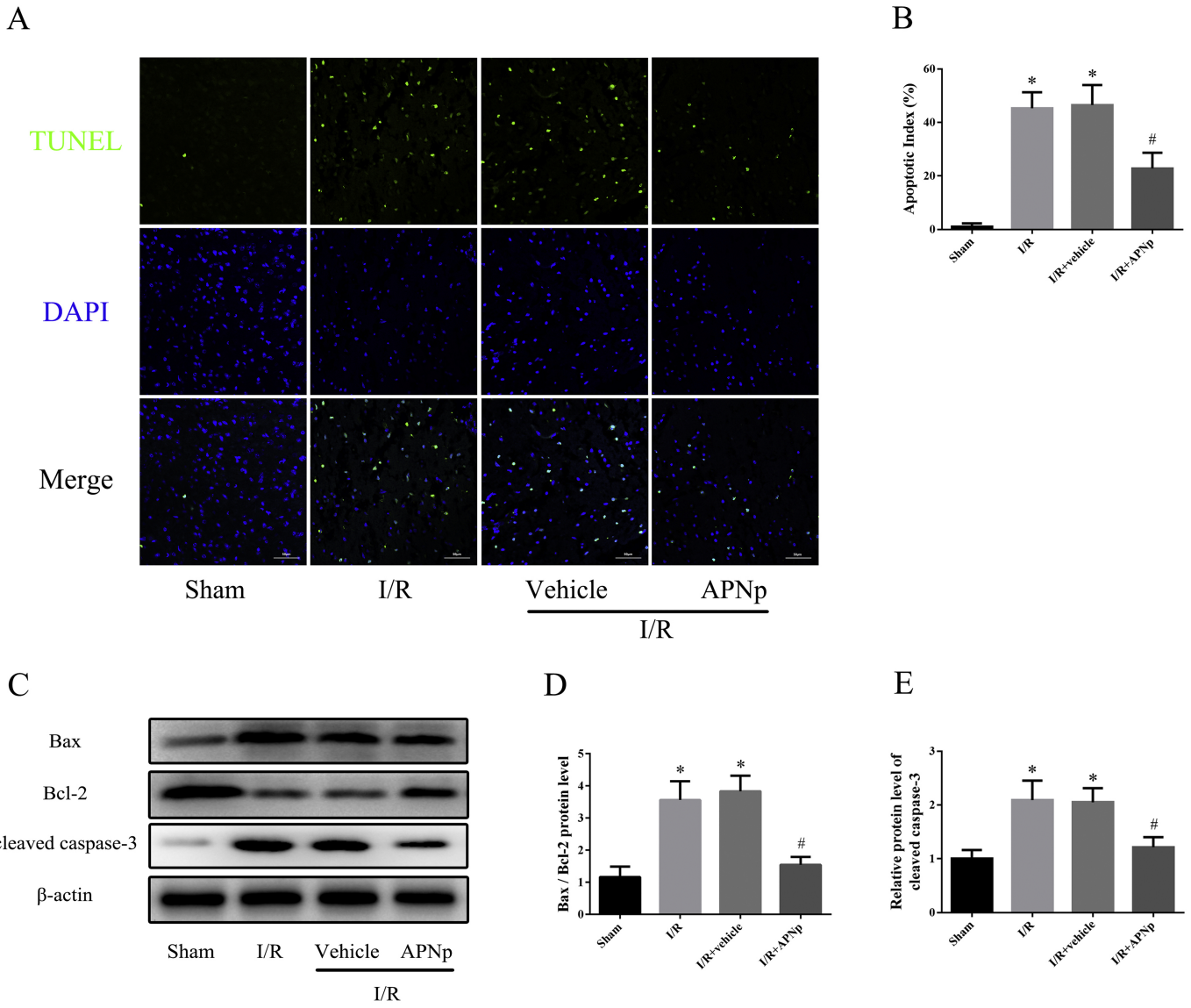
A
TUNEL
DAPI
Merge
Sham
I/R
Vehicle
APNp
I/R
B
Apoptotic Index (%)
60
40
20
0
*
*
#
Sham
I/R
I/R+vehicle
I/R+APNp
C
Bax
Bcl-2
cleaved caspase-3
β-actin
Sham
I/R
Vehicle
APNp
I/R
D
Bax / Bcl-2 protein level
5
4
3
2
1
0
*
*
#
Sham
I/R
I/R+vehicle
I/R+APNp
E
Relative protein level of cleaved caspase-3
3
2
1
0
*
*
#
Sham
I/R
I/R+vehicle
I/R+APNp

Figure 2

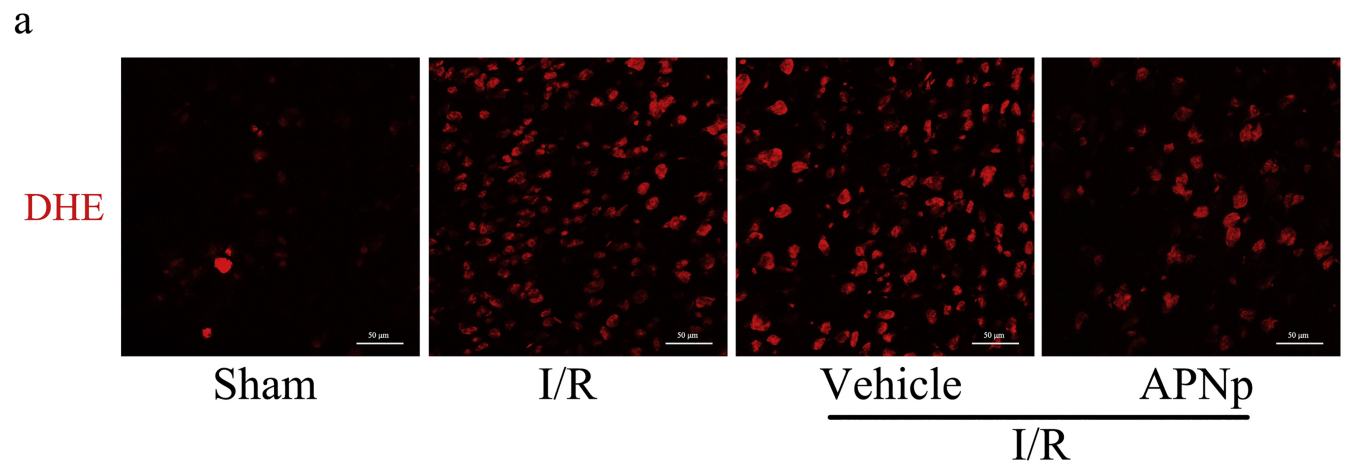
a
DHE
50 μm
Sham
I/R
Vehicle
APNp
I/R

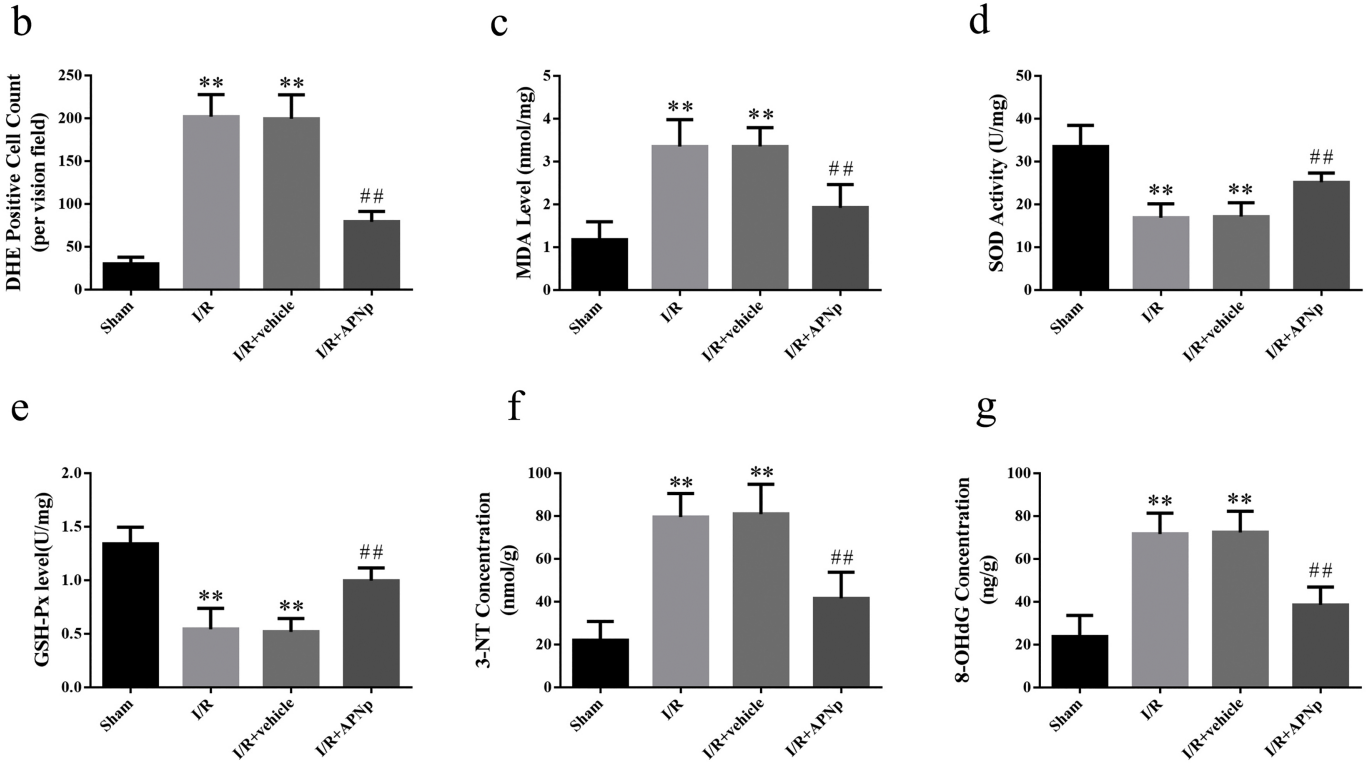
b
DHE Positive Cell Count (per vision field)
c
MDA Level (nmol/mg)
d
SOD Activity (U/mg)
e
GSH-Px level(U/mg)
f
3-NT Concentration (nmol/g)
g
8-OHdG Concentration (ng/g)
Sham
I/R
I/R+vehicle
I/R+APNp
**
##

Figure 3

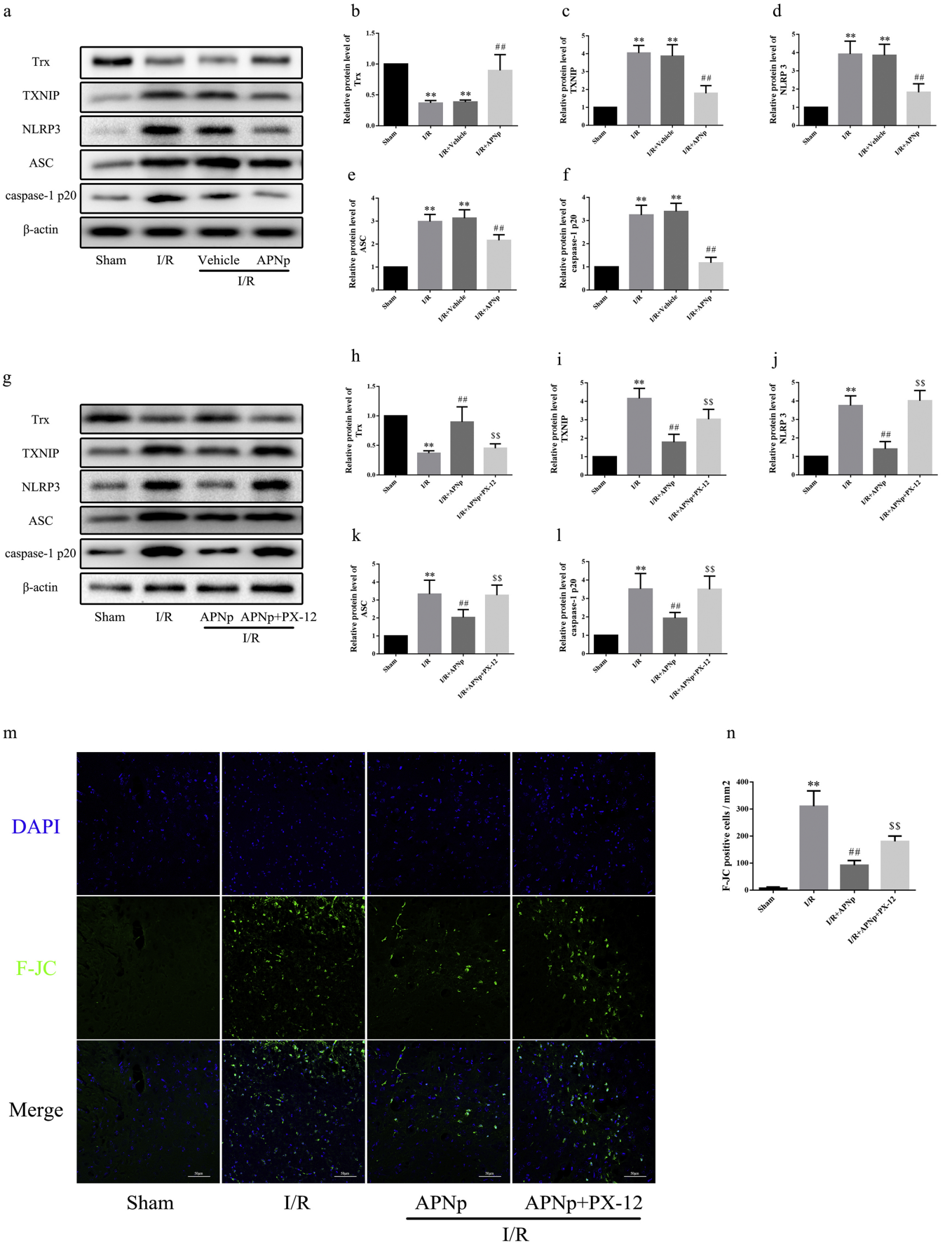
a
Trx
TXNIP
NLRP3
ASC
caspase-1 p20
β-actin
Sham
I/R
Vehicle
APNp
I/R
b
Relative protein level of Trx
c
Relative protein level of TXNIP
d
Relative protein level of NLRP 3
e
Relative protein level of ASC
f
Relative protein level of caspaase-1 p20
Sham
I/R
I/R+Vehicle
I/R+APNp
g
Trx
TXNIP
NLRP3
ASC
caspase-1 p20
β-actin
Sham
I/R
APNp
APNp+PX-12
I/R
h
Relative protein level of Trx
i
Relative protein level of TXNIP
j
Relative protein level of NLRP 3
k
Relative protein level of ASC
l
Relative protein level of caspaase-1 p20
Sham
I/R
I/R+APNp
I/R+APNp+PX-12
m
DAPI
F-JC
Merge
Sham
I/R
APNp
APNp+PX-12
I/R
n
F-JC positive cells / mm2
Sham
I/R
I/R+APNp
I/R+APNp+PX-12

Figure 4

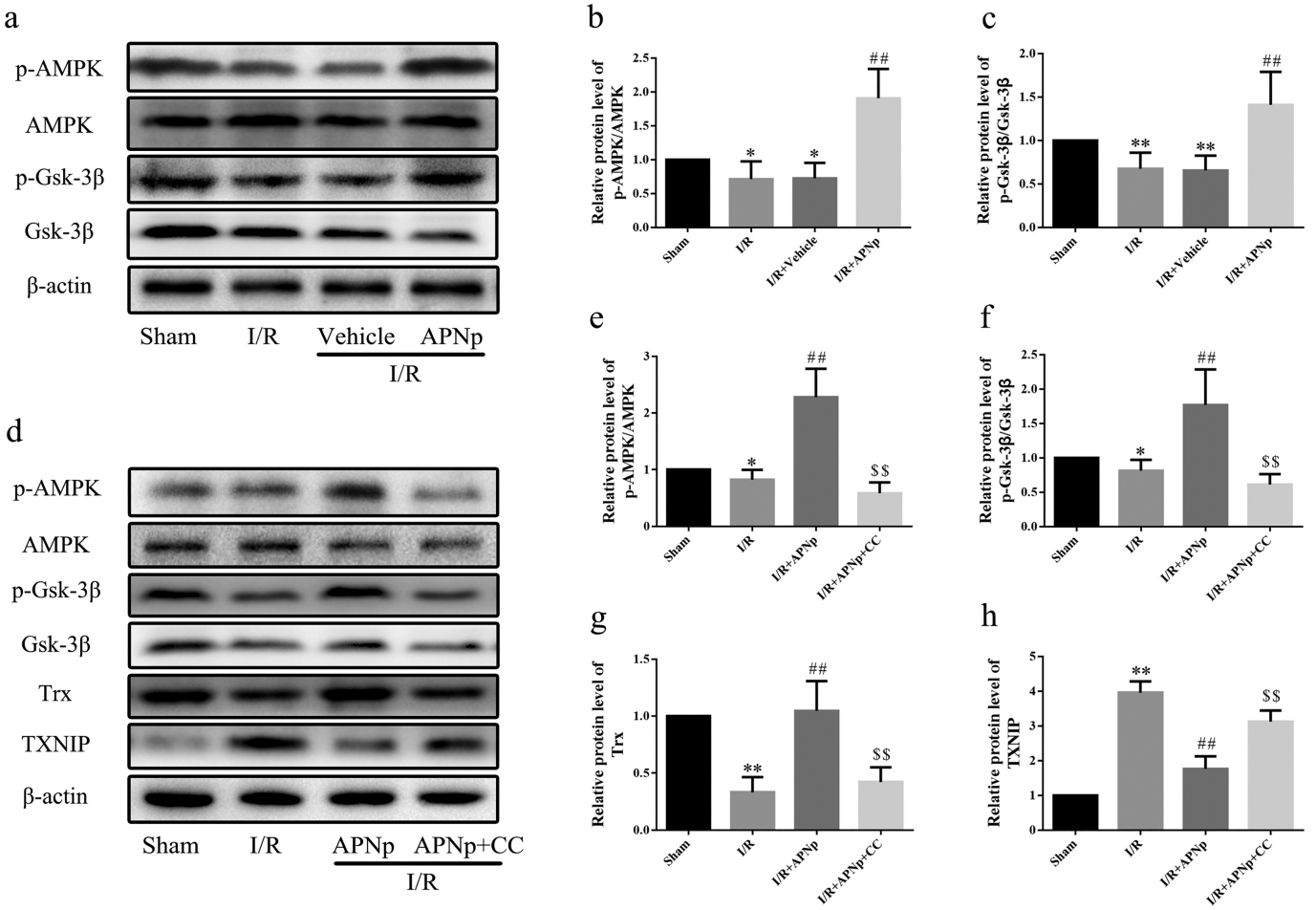
a
p-AMPK
AMPK
p-Gsk-3β
Gsk-3β
β-actin
Sham
I/R
Vehicle
APNp
I/R
b
Relative protein level of p-AMPK/AMPK
c
Relative protein level of p-Gsk-3β/Gsk-3β
Sham
I/R
I/R+Vehicle
I/R+APNp
d
p-AMPK
AMPK
p-Gsk-3β
Gsk-3β
Trx
TXNIP
β-actin
Sham
I/R
APNp
APNp+CC
I/R
e
Relative protein level of p-AMPK/AMPK
f
Relative protein level of p-Gsk-3β/Gsk-3β
g
Relative protein level of Trx
h
Relative protein level of TXNIP
Sham
I/R
I/R+APNp
I/R+APNp+CC

Figure 5

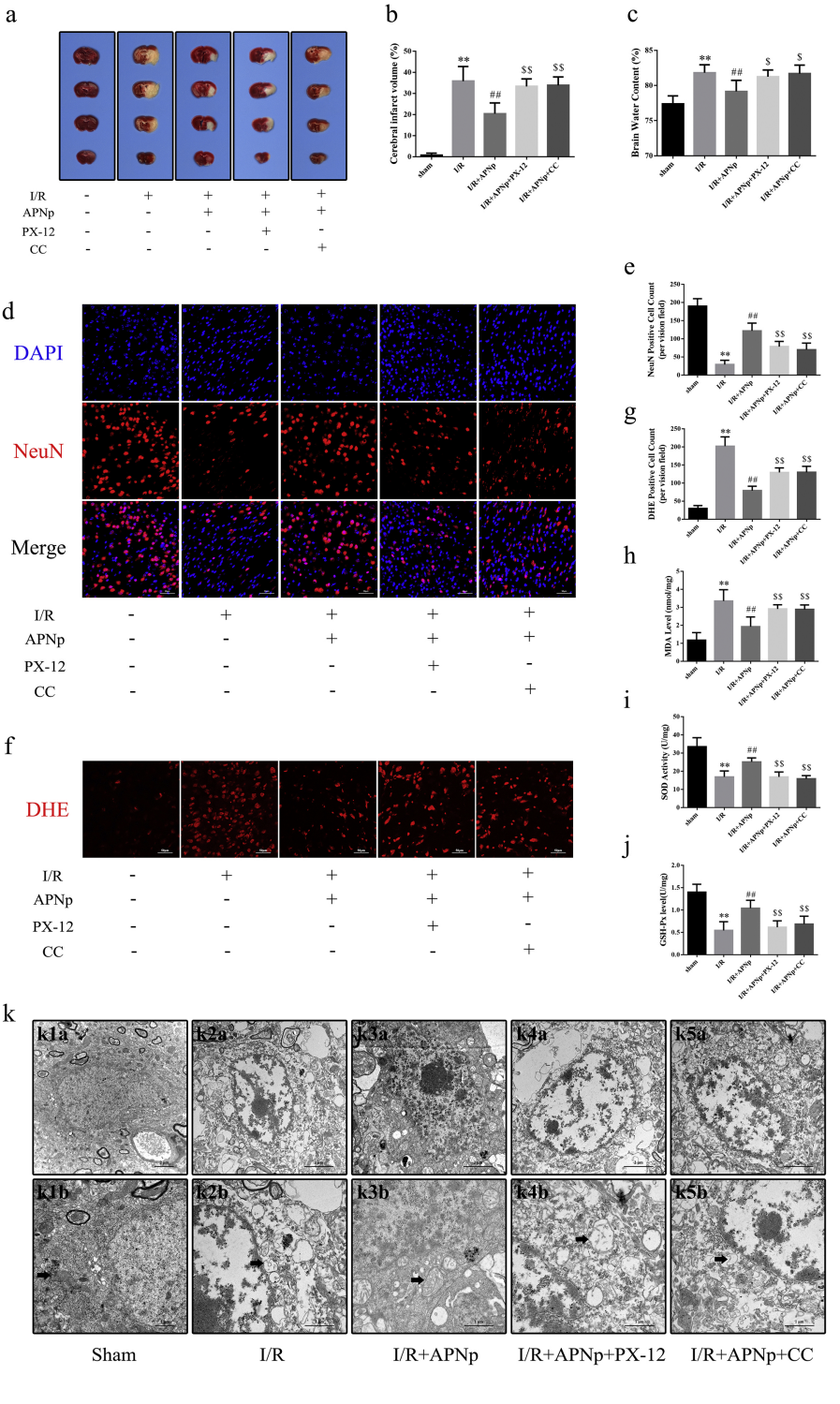
a
I/R - + + + +
APNp - - + + +
PX-12 - - - + -
CC - - - - +
b
Cerebral infarct volume (%)
sham
I/R
I/R+APNp
I/R+APNp+PX-12
I/R+APNp+CC
c
Brain Water Content (%)
d
DAPI
NeuN
Merge
e
NeuN Positive Cell Count (per vision field)
f
DHE
g
DHE Positive Cell Count (per vision field)
h
MDA Level (nmol/mg)
i
SOD Activity (U/mg)
j
GSH-Px level(U/mg)
k
k1a
k2a
k3a
k4a
k5a
k1b
k2b
k3b
k4b
k5b
Sham
I/R
I/R+APNp
I/R+APNp+PX-12
I/R+APNp+CC
l
Bcl-2
Bax
active caspase 3
β-actin
m
Relative protein level of Bax/Bcl-2
n
Relative protein level of active caspase-3

Figure 6

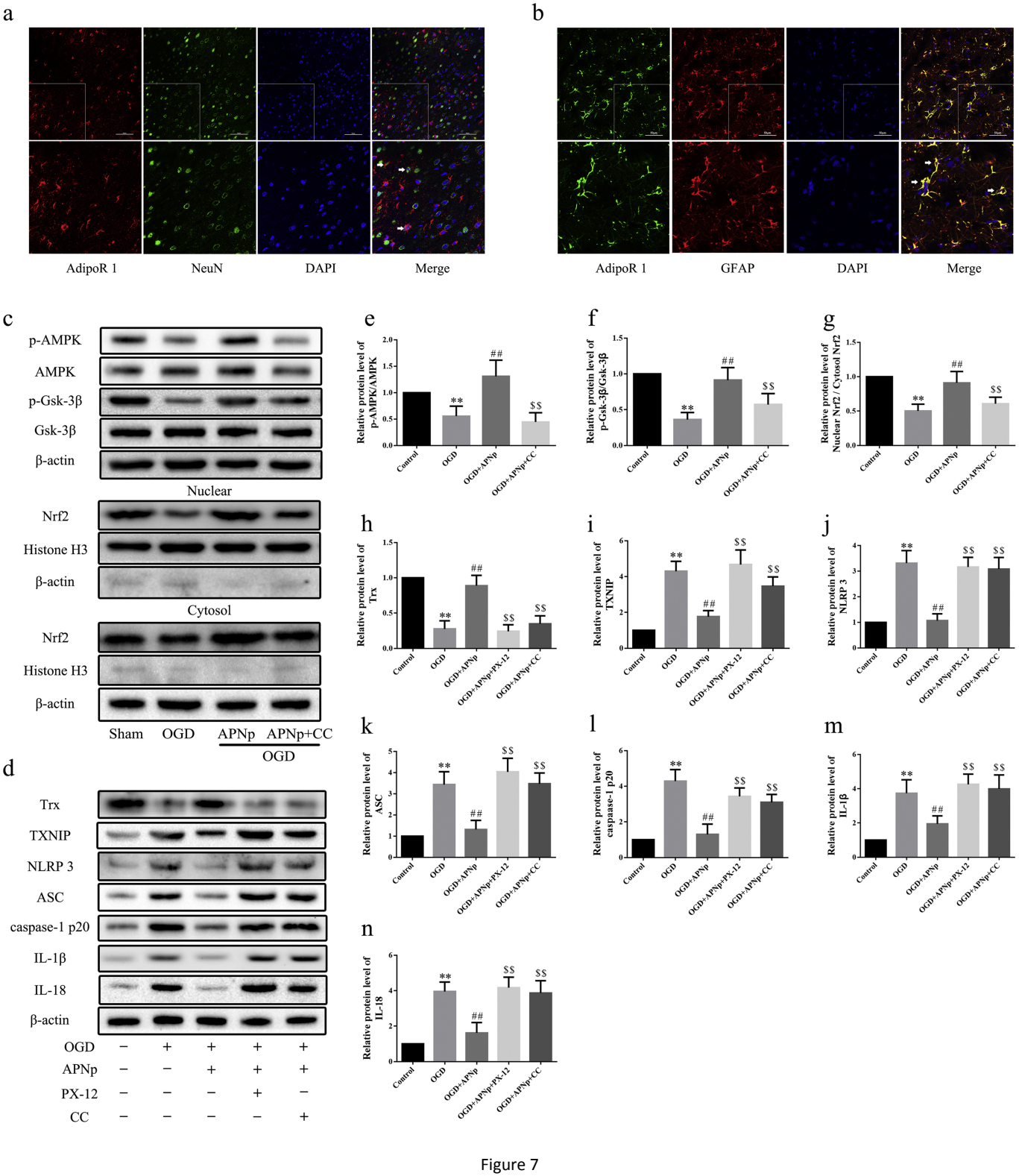
a
AdipoR 1
NeuN
DAPI
Merge
b
AdipoR 1
GFAP
DAPI
Merge
c
p-AMPK
AMPK
p-Gsk-3β
Gsk-3β
β-actin
Nuclear
Nrf2
Histone H3
β-actin
Cytosol
Nrf2
Histone H3
β-actin
Sham
OGD
APNp
APNp+CC
OGD
d
Trx
TXNIP
NLRP 3
ASC
caspase-1 p20
IL-1β
IL-18
β-actin
OGD − + + + +
APNp − − + + +
PX-12 − − − + −
CC − − − − +
e
Relative protein level of p-AMPK/AMPK
f
Relative protein level of p-Gsk-3β/Gsk-3β
g
Relative protein level of Nuclear Nrf2 / Cytosol Nrf2
h
Relative protein level of Trx
i
Relative protein level of TXNIP
j
Relative protein level of NLRP 3
k
Relative protein level of ASC
l
Relative protein level of caspaase-1 p20
m
Relative protein level of IL-1β
n
Relative protein level of IL-18
Control
OGD
OGD+APNp
OGD+APNp+PX-12
OGD+APNp+CC
**
##
$$

Figure 7

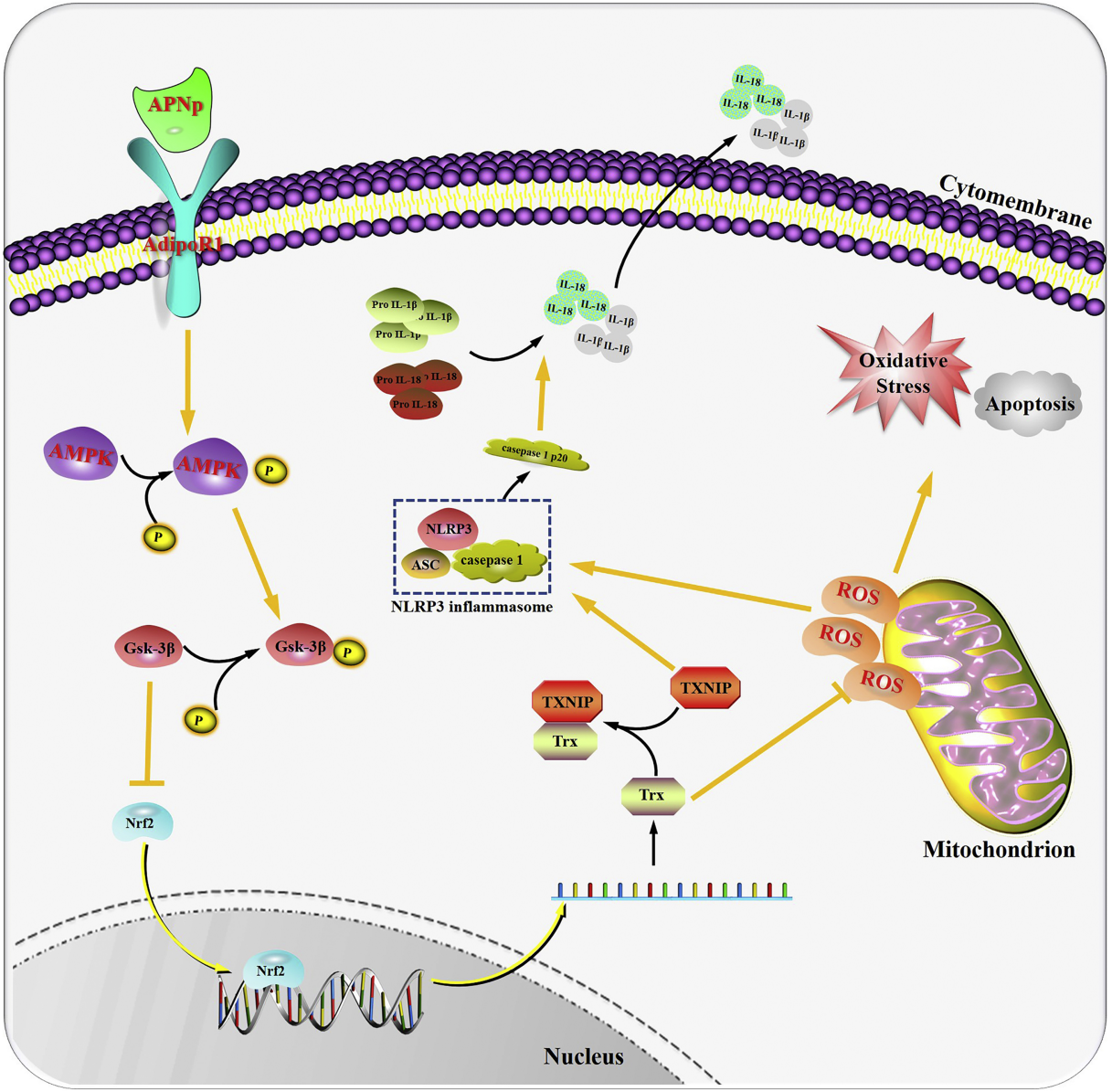
APNp
AdipoR1
Cytomembrane
IL-18
IL-1β
Pro IL-1β
Pro IL-18
AMPK
P
Gsk-3β
Nrf2
casepase 1 p20
NLRP3
ASC
casepase 1
NLRP3 inflammasome
Oxidative Stress
Apoptosis
ROS
TXNIP
Trx
Mitochondrion
Nucleus

Figure 8